Development of Dual-Frequency Injection-Locked Continuous-Wave Ti: Sapphire Laser and Its Applications to Nonlinear Optical-Phenomena

Trivikramarao Gavara

The University of Electro-Communications

Tokyo, Japan

September 2017

Development of Dual-Frequency Injection-Locked Continuous-Wave Ti: Sapphire Laser and Its Applications to Nonlinear Optical-Phenomena

by

Trivikramarao Gavara

A dissertation submitted in partial fulfillment of the requirements for the degree of Doctor of Philosophy

to

Department of Engineering Science
Graduate School of Informatics and Engineering
The University of Electro-Communications
Chofu, Tokyo, Japan

September 2017

Development of Dual-Frequency Injection-Locked Continuous-Wave Ti: Sapphire Laser and Its Applications to Nonlinear Optical-Phenomena

Trivikramarao Gavara

Approved by

Chair of Committee:
PROF. Masayuki KATSURAGAWA
Department of Engineering Science
University of Electro-Communications

Committee Members:
PROF. Ken'ichi NAKAGAWA
Institute of Laser Science
University of Electro-Communications

PROF. Kaoru MINOSHIMA
Department of Engineering Science
University of Electro-Communications

PROF. Akira SHIRAKAWA
Institute of Laser Science
University of Electro-Communications

PROF. Mitsuru MUSHA
Institute of Laser Science
University of Electro-Communications

Dedicated to my Parents

Satyannarayana and Mutyamamma

Acknowledgments

The completion of my thesis wouldn't have been possible without the encouragement and help of many wonderful people.

First and foremost, I wold like to acknowledge my supervisor Prof. Katsuragawa for all the guidance and support throughout the course. I was very lucky to join in his group, thank you for giving me an invaluable chance to work in such a highly scientific environment. He is very nice person and a great teacher I have ever seen. I am very much thankful to him.

I would like to thank my co-supervisor Prof. Nakagawa for his comments, suggestions, and for review my thesis. Also, I would like to express my thanks to Prof. Minoshima, Prof. Shirakawa, and Prof. Musha for their valuable advice and comments in improving my thesis.

I want to give my special thanks to Dr. Ohae, Dr. Yoshii, Dr. Zheng and Dr. Nakano for their help in the lab. Also, I would like to acknowledge Yoshizaki, Fujimura, Liu, Sato, Trigubov Dmitry, Chuan, Sasaki, Ohashi and Kawashima for their wonderful companion during my Ph.D course.

I would like to acknowledge my college and friend Dr. Nurul Sheeda Shuhaimi for her help in the laboratory and in understanding the Japanese language. We had joined in the laboratory at the same time and worked together for more than four years. During this time she helped me in many ways, I am very much thankful to her.

I am greatly indebted Center For International Programs and Exchange faculty Prof. Ikeda and other teachers who taught me basics in Japanese language and their support during my stay at UEC. Also, I would like to acknowledge Prof. T. Hamano and Prof. Ikeda for their support and help during my stay at UEC.

I would like to thank all the secretaries Miyake San, Izumi San, Kaga San for the administrative support during my course.

I would like to acknowledge Dr. Kanaka Raju for introduced me to Prof. Katsuragawa and for his guidance during my studies. He is one of the person by whom I was inspired and selected the research as the career.

I would like to acknowledge many wonderful friends and great researchers that I have met at UEC; Dr. Kali, Dr. Ramachandra, Dr. Srinivas, Dr. Gangi Reddy, Dr. Manasa, Dr. B. M. Manoj, Dr. Manoj Das, Dr. Dinesh, Dr. Sanjay, Rakesh, Jameesh and Shafi for their continuous support and encouragement throughout my Ph.D course is an unforgettable.

I would like to acknowledge Dr. Halubai Sekar, for his support and guidance during my stay in Japan. I am very much thankful to him.

I have obtained my master degree in physics from the University of Hyderabad and I would like to thank the Professors from school of physics , who taught me the basics of the Physics. I am very much thankful to Prof. D. Narayana Rao, for gave an opportunity to start my research career in his lab and for taught me the basic things in the experimental physics.

I would like to acknowledge many wonderful people that I have met at the lap of UOH; Surya, Eswar Reddy, Venkatesh, Sriram, Jagadeesh Bommi, Appala Naidu, Sravan Kumar, Praneetha, Anna Poorna and all my classmates for their support and encouragement during my good and bad times. I hope, we will continue our friendship to the rest of our life.

I am grateful to all my friends in my village Dabbi Raju Peta; Vara Prasad, Naga Raju, Arjun, Srinivas, Kanaka Raju and Ramana for being with me and for support-

ing my strength and determination.

I would like to acknowledge my friends Prasad, Praveen, Laxman, Ramesh, Hyma, Padmanabha Swamy and Rajesh for their continuous support and help.

Most importantly, I would like to thank my parents, brother and sisters for their love and support throughout my life. I feel very lucky to have such a beautiful family, and being away from them was the most difficult part of living in Japan. Although I don't tell them often, I love my family very much.

Development of Dual-Frequency Injection-Locked Continuous-Wave Ti: Sapphire Laser And Its Applications to Nonlinear Optical-Phenomena

Abstract: This thesis describes the development of dual-frequency injection-locked (DFIL) continuous-wave titanium-sapphire laser and its applications in the study of cavity based stimulated Raman scattering and also in the generation of phase locked harmonics by optical frequency division technology to demonstrate the continuous wave based arbitrary optical wave form synthesis. At first, the DFIL laser fundamental properties such as single longitudinal mode profile, single transverse mode, and practical power stability were characterized.The DFIL laser delivers a maximum of 2.8 W total output power at a 10 W pump power. As the advanced abilities, desirable two frequency separation (1 THz to 10 THz) and well controlled relative output power ratios as a function of injection seed powers over a wide dynamic range were demonstrated.

As an application of the DFIL laser, CW laser based stimulated Raman scattering in the para- H2 gas medium was studied. For this purpose, Ti: sapphire laser output was coupled to the high finesse optical cavity and observed multiple Stokes and anti-Stokes rotational Raman components of the para-H_2 J=0 to J=2 rotational transition. Efficient anti-Stokes generation through four wave mixing process was obtained by controlling the gas density for a fixed mirror dispersion which was introduced from its dielectric coating.

The output of the Ti: sapphire laser was coupled to an array of periodically poled lithium niobate (PPLN) wave guides, together with another IR frequency and generated phase locked five harmonics with a frequency spacing of 125 THz by the optical division technology. These phase locked harmonics were synthesized to obtain the arbitrary optical wave form by utilizing the novel technique of the freely controlled optical phases and amplitudes by controlling the thickness of the transparent dispersive media in the optical path. In this way, an ultrashort pulse train with a repetition rate of 125 THz and a pulse duration of 1.6 fs was obtained.

Table of Contents

List of Figures **iv**

1 Introduction **1**

1.1 Literature and overview 1

1.2 Thesis overview 4

2 Dual-Frequency Laser System **9**

2.1 Introduction 9

2.2 Injection-locking and locking range 10

2.3 DFIL laser system 11

2.3.1 Master cavity 12

2.3.2 Seed lasers system 13

2.3.3 Power oscillator 14

2.4 Conclusions 17

3 Dual-frequency laser characteristics **19**

3.1 Introduction 19

3.2 Seed frequencies stabilization 19

3.3 Stabilization of power oscillator for simultaneous two frequency resonance 21

3.4 Simultaneous two frequency laser oscillation 23
3.4.1 Free run suppression and power spectrum 24
3.5 Fundamental features of the DFIL laser 26
3.5.1 Spectral purity 26
3.5.2 Spatial mode purity (M^2 measurement) 28
3.5.3 Output power stability 30
3.6 Advanced features of the DFIL laser 32
3.6.1 Arbitrary frequency separation 32
3.6.2 Relative power controllability 34
3.7 Conclusions 35

4 Study of Raman based molecular modulator 38
4.1 Introduction 38
4.2 Theory of Raman based molecular modulator 39
4.3 Experimental system 43
4.4 Dispersion effect on coherent Raman sidebands generation 44
4.5 Results and discussions 47
4.6 Conclusions 54

5 Ultrafast optical pulse train at 125 THz repetition rate based on the optical frequency division technology 57
5.1 Introduction 57
5.2 Concept of optical frequency division 58
5.3 Overview of amplitude and phase manipulations 59
5.4 Experimental system 60
5.5 Results and discussion 62
5.6 Conclusions 67

6 Summary and future prospects 70
6.1 Summary 70
6.2 Future prospects 72

A Simultaneous two frequency resonance of power oscillator cavity **74**

B Cavity mirrors reflectivity: **76**

C Mirror coatings **78**

List of Publications **80**

Conference contributions-International **81**

Conference contributions-Domestic **83**

List of Figures

1.1 Extreme laser light sources and their applications 2

2.1 Illustration of the injection locking range; A modified version of the A. E. Siegman, Lasers (1986) 11

2.2 Illustration of the master cavity. M1 and M2 are highly reflective cavity mirros; PZT, piezoelectric transducer. 12

2.3 Illustration of the seed lasers system. ECDL, external-cavity controlled diode laser; Iso, inline isolator; TA, tapered amplifier; EOM, electro-optic modulator; PD, photo-detector; GL, glan laser polarizer; PS, phase shifter; LO; local oscillator; Mix, radio frequency mixer; SA, servo amplifier 13

2.4 Illustration of the Ti:sapphire power oscillator. MML, mode matching lens; M, mirror; PZT, piezoelectric transducer; R, reflectivity; PM, pico motor. 14

2.5 Photograph of Ti: sapphire bow-tie ring cavity power oscillator . . . 15

2.6 Illustration of DFIL Ti:sapphire laser total experimental system. PD2 and PD3, photo-detector; SA, servo-amplifier; FG, function generator; GLP; Glan laser polarizer 17

3.1 (a) and (b) are the PDH error signals corresponding to the frequencies ω_1 and ω_2. The black curves are the error signals while sweeping the frequency around the cavity resonance and the red curves are the error signals after the frequency stabilization 20
3.2 Simultaneous stabilization of the seed frequencies to the power oscillator cavity. Black and red Lorentzian curves are the longitudinal modes of the power oscillator cavity corresponds to the frequencies ω_1 and ω_2. 22
3.3 Dual-frequency injection-locked oscillation. The red curves are the injection locked simultaneous dual-frequency oscillation, the gray curve is the free running oscillation and the dotted blue curves represent the seed frequencies. 23
3.4 Free-running suppression as a function of total injection seeded power. The green circles and red triangles are the free-running suppression in the cases of single and dual-frequency injection locking states respectively. 24
3.5 Dual frequency output power as a function of the pump power. The black squares and the red circles are the total output powers in the case of free running and injection locked states respectively. 26
3.6 Longitudinal mode analysis with a Fabry-Perot spectrum analyzer. The red and the gray curves are the longitudinal modes in the case of injection locked and free-running states respectively. 27
3.7 Beat note between the injection locked output frequency and the frequency shifted seed frequency 28
3.8 Analysis of spatial mode purity by M^2measurement. The red circles and black triangles represent the beam diameters corresponding to the frequencies ω_1 and ω_2 respectively 29
3.9 Output power stability of the DFIL laser a) short time duration power stability observation and b) relatively long time duration power stability observation 31
3.10 Arbitrarily separated frequency pairs. 32

3.11 Controllable relative power ratios as the function of the injected seed powers 34
3.12 Arbitrary combinations of the output power 35

4.1 Energy level diagram of far-off resonant three level system driven by two strong laser fields. 39
4.2 Experimental system to study the Raman sideband generation. W, window; M_1 and M_2; cavity mirrors, BS; beam splitter, OMA; optical multi-channel analyzer. 44
4.3 Effect of frequency dependent free spectral range (FSR) in the generation of Stokes and anti-Stokes fields inside the Raman cavity 46
4.4 Raman medium dispersion and offresonant of Stokes and anti-Stokes . 48
4.5 Multiple rotational Raman sideband generation by single frequency driving (784nm) 49
4.6 Density dependent Raman sideband generation by single frequency driving (806 nm) 50
4.7 Dispersion introduced by the para-H2 gas and cavity mirrors. 51
4.8 Dual-frequency pumped Raman generation 52
4.9 Temperature dependent population density of Para-H_2 rotational energy levels 53
4.10 Raman generation in Para hydrogen using multiple rotational transitions 54

5.1 Conceptual schematic of optical frequency division technique 58
5.2 Schematic of arbitrary manipulation of amplitude and phases of a discrete frequencies 59
5.3 Illustration of phased locked harmonics generation system and optical pulse train generation experimental system 61
5.4 Harmonic powers before and after amplitude manipulation 63
5.5 Relative phases of harmonics before and after phase manipulation . . 65
5.6 Reconstructed waveform by using the measured phases and amplitudes 66

A.1 Deviation from simultaneous two frequency resonance of the power oscillator cavity as function of the prism insertion length. a) , b) and c) are the resonance measurements corresponding to the frequency pairs (783.8849 nm, 806.2823 nm), (800.0590 nm, 806.2885 nm), (801.1395, 803.0041) respectively 75

B.1 Raman cavity mirror refelectivities; specifications given by Layertec Ltd 77

C.1 Group delay dispersion of the cavity mirrors under one reflection . . . 79

CHAPTER 1

Introduction

1.1 Literature and overview

Since the first demonstration of the laser in 1960 by Theodore Harold Maiman, there have been significant advances in the laser light sources. Development of the laser light sources along with the optical technology, not only enhances the progress of the optical science, but also brings the revolutionary changes in the industry. In the past 50 years there were developed many extreme laser light sources such as single frequency laser, ultra high intense laser, ultra-short pulsed laser, ultra fast laser, and short wavelength laser. Development of the single frequency laser source enabled the study of the high resolution precision spectroscopy, laser cooling [1], Bose-Einstein condensation and also it plays an important role in the demonstration of the highly standardize optical clocks [2] and in the detection of the gravitational waves [3]. Development of the ultra-short pulsed lasers with a time scale of a few femto-seconds (10^{-15}) [4] to atto-seconds (10^{-18}) shows the way to observe the ultra-fast processes in the nature such as the motion of the electrons and fast chemical reactions. Another extreme laser source is the short wavelength laser, such as vacuum

ultraviolet, extreme ultraviolet and coherent X-ray laser sources. These laser sources have strong applications in the industry as well as in the optical science such as in the lithography (development of the ultra-small structures such as micro electronics). Also, these lasers have good number of applications in the biology (in the study of proteins) and in the medicine (ophthalmology). Another extreme laser source is the ultrahigh power lasers, which enables the laser based particle accelerators, high harmonic generation and laser plasma. Such a huge area of optical science is established in the past 50 years, because of the continuous progress in the laser technology. Laser light sources and some of their applications are shown in figure 1.

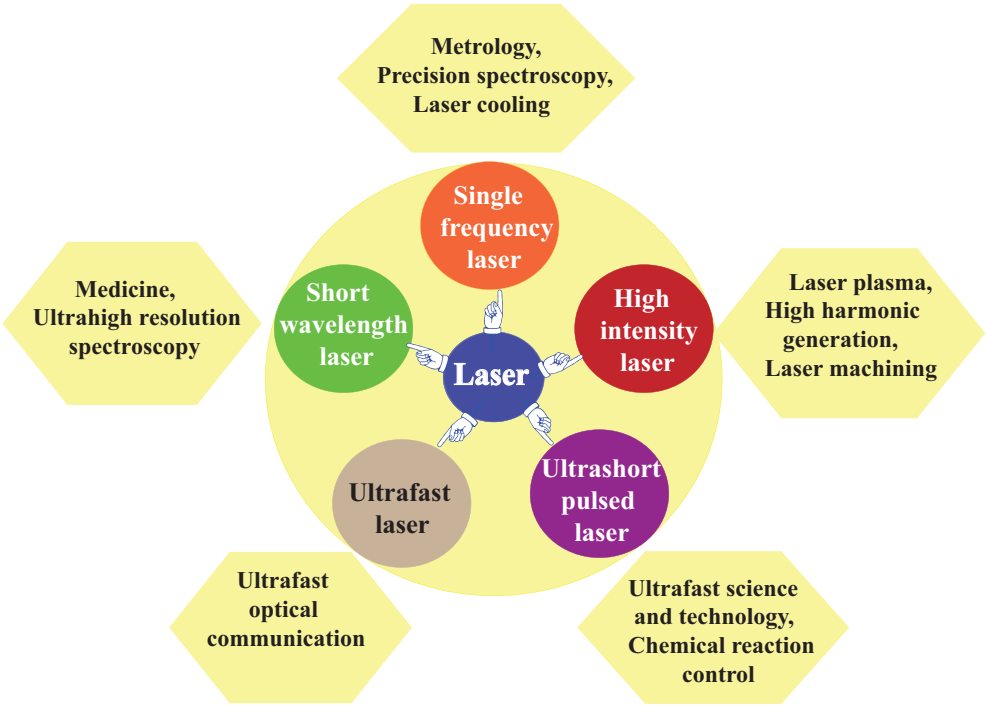

Figure 1.1: Extreme laser light sources and their applications

Here, we have developed the conceptual design of an injection-locked dual-frequency laser for the first time and realized the dual frequency laser oscillation. The advantages with this laser are good spatial overlap between the two frequency beams, controllable relative powers and arbitrary separation of the frequency pairs. These features are crucial for many nonlinear optical phenomena when there is need of two or more frequencies. Development of such a laser source makes the experiments easy

in terms of optical alignments such as spatial overlap of the multiple frequency beams. The dual-frequency laser source is realized with the aid of injection locking technique.

So far, single frequency injection locked operation in various kinds of laser systems such as YAG lasers and Ti:sapphire lasers etc., have been reported [5–9]. Few of the dual-frequency lasers were reported, in the diode lasers by two longitudinal mode operation [10], in the Nd:YAG by injection seeded [11], and in the Ti:sapphire lasers by self seeding technique and through intra-cavity wavelength selective elements [12, 13] etc., There are few reports on the two frequency injection locked laser operation in the nano-second pulsed regime [14–17]. There are no reports on dual-frequency injection-locked operation of continuous wave lasers. We proposed a method to demonstrate the stable two frequency laser oscillation from a single laser cavity. The key techniques are injection seeding and locking the cavity length for simultaneous two frequency resonance. For this, we choose the Ti: sapphire power oscillator, because of its wide frequency bandwidth from 700-1100 nm [18], and good optical to optical conversion efficiency.

Multiple frequency lasers with arbitrary frequency separation and narrow line width have good number of applications in the study of various optical phenomena such as, nonlinear optical processes in isolated atomic or molecular systems [19–21], four wave mixing process [22], THz generation [23, 24], atom interferometry, simultaneous cooling and trapping of multiple atomic spices [25], atmospheric science, precision spectroscopy and differential absorption LIDAR [26–28]. All these studies are required more than one frequency with high spectral purity.

Although the dual frequency laser system is a little complex, it has many advantages apart from its compact size, like spatial overlap of the multiple frequency beams, similar divergence pattern and controllable output powers of the two frequencies. These features are crucial for the many nonlinear optical experiments and difficult to realize by simply combining the two independent laser beams in the free

space. Injection locked lasers have many advantages compared with other laser systems such as master oscillator power amplifier (MOPA) laser systems. MOPA lasers are simple in nature but it includes the distorted beam profile from the mode mismatch between the master laser and amplifier, and thermally induced birefringence, which causes for the depolarization. Also, the output of the MOPA lasers includes the amplified spontaneous emission which is not acceptable for many optical experiments. Even though it has a simple operation, because of these drawbacks one can not use, if these parameters effect the physical measurements. Injection locked lasers over come these draw backs and enhance the applications.

1.2 Thesis overview

This thesis mainly deals with development of a dual frequency injection locked laser and its applications in the study of Raman based molecular modulator by using para-H_2 gas and cavity enhancement technique. It also presents an application of the injection locked single frequency laser in the generation of the continuous wave laser based phase locked harmonics by using the optical frequency division technique to realize the 125 THz repetition rate ultrafast optical pulse train by manipulating the relative phases and amplitudes of the phase locked harmonic frequencies.

Chapter2 provides the full details of the dual-frequency injection locked laser (DFIL) system. The main components of the DFIL laser such as master cavity, seed lasers system, Pound-Drever-Hall locking system and bow-tie ring cavity power oscillator are described in this chapter.

Chapter3 describes the performance of the DFIL laser system. The laser fundamental features like single frequency, single transverse mode profiles are characterized by analyzing with the scanning Fabry-Perot cavity and by measuring the M^2 factors and the results are discussed. Also, we present the laser practical power stability in

the short time scale and relatively long time scales. DFIL laser free-running power suppression as a function of injection seed power is presented. As the advanced features, arbitrary frequency separation of the two frequencies from 1THz to 10THz are presented with the injection locking technique. Also, we present the controllabilty of the relative output power ratios of the injected frequencies as a function of the injection seed powers.

In **chapter4**, an application of the dual-frequency injection-locked laser in the study of the continuous wave laser based molecular modulator is described. Generation of the coherent Raman sidebands in the para-H_2 gas medium by utilizing the optical cavity enhancement technique is studied. We present the multiple Stokes generation by driving the para-H_2 medium with a single frequency laser corresponding to the rotational transition J=0 to J=2 . We discuss the requirements and their possibilities to generate broad band coherent stokes and anti-stokes through cavity enhancement technique.

In **chapter5**, an application of the single frequency injection locked laser in the generation of phase locked harmonics is described. Importance of the high power master laser in the generation of the phase locked high harmonics using the optical frequency division technique is narrated. Also we report the arbitrary manipulation of the relative phases and amplitudes of the harmonic frequencies by simply placing the dispersive elements in the optical path and by controlling their thicknesses. Realization 125 THz ultrafast optical pulse train based on the continuous wave harmonic frequencies is described

In **chapter6**, we summarize the main results of the thesis and discuss the future prospects of this research work.

Bibliography

[1] C. S. Adams, and E. Riis, "Laser cooling and trapping of neutral atoms", Prog. Quant. Elec. **21**, 1-79 (1997).

[2] Nils Nemitz, Takuya Ohkubo, Masao Takamoto, Ichiro Ushijima, Manoj Das, Noriaki Ohmae and Hidetoshi Katori, " Frequency ratio of Yb and Sr clocks with $5 * 10^{-17}$uncertainty at 150 seconds averaging time", Nat. Photon. **10** , 258-261 (2016)

[3] B. P. Abbott et al, "Properties of the binary black hole merger GW150914", Phy. Rev. Lett. **116** , 241102 (2016).

[4] J. DeMaria, C. Ferrar, and G. E. Danielson, "Self modelocking of lasers with saturable absorbers", J. Appl. Phys. Lett. **8** , 22 (1966).

[5] A. D. Farinas, E. K. Gustafson, and R. L. Byer, "Design and characterization of a 5.5 W , cw, injection-locked, fiber-coupled, laser-diode-pumped Nd:YAG miniature-slab laser", Opt. Lett. **19**, 114-116 (1994).

[6] M. Musha, K. Nakagawa, K. Ueda, "Wideband and high frequency stabilization of an injection-locked Nd:YAG laser to a high-finesse Fabry–Perot cavity", Opt. Lett. **22**, 1177-1179 (1997).

[7] E. A. Cummings, M. S. Hicken, and S. D. Bergeson, "Demonstration of a 1-W injection-locked continuous-wave titanium:sapphire laser", Appl. Opt. **41**, 7583-7587 (2002).

[8] K. Takeno, T. Ozeki, S. Moriwaki, and N. Mio, "100 W, single-frequency operation of an injection-locked Nd:YAG laser", Opt. Lett. **30**, 2110-2112 (2005).

[9] S. –W. Chiow, S. Herrmann, H. Muller, S. Chu, "6 W, 1 kHz linewidth, tunable continuous-wave near-infrared laser", Opt. Exp. **17**, 5246-5250 (2009).

[10] S. lio, M. Suehiro, T. Hirata and T. Hidaka, "Two-longitudinal-mode laser diodes", IEEE Phot. Tech. Lett. **7**, 959-961 (1995).

[11] T. D. raymond and A. V. Smith, "Two-frequency injection-seeded Nd:YAG laser", IEEE J. Quantum Electron. **31**, 1734-1737 (1995).

[12] R. Scheps and J. F. Mayers, "Doubly resonant Ti:sapphire laser", IEEE Phot. Tech. Lett. **4**, 1-3 (1992).

[13] M. Gorris-Neveux, M. Nenchev, R.Barbe, and J. C. Keller, "A two wavelength, passively self-injecion locked, CW Ti^{+3}:Al_2O_3 laser", IEEE J. Quantum Electron **31**, 1253-1260 (1995).

[14] M. Katsuragawa and T. Onose, "Dual-wavelength injection-locked pulsed laser", Opt. Lett. **30**, 2421-2423 (2005).

[15] T. Onose and M. Katsuragawa, "Dual-wavelength injection-locked pulsed laser with highly predictable performance", Opt. Exp.**15**, 1600-1605 (2007).

[16] T. Nakano, K. Koizumi, T. Onose, K. Abe, and M. Katsuragawa, "Dual-frequency injection-locked nanosecond pulsed laser with arbitrary combination of two oscillation frequencies", Opt. Express **18**, 26409-26416 (2010).

[17] Y. Fujii and M. Katsuragawa, "Dual-frequency pulsed laser with an accurate gigahertz-beat note", Opt. Exp.**32**, 3065-3067 (2007).

[18] P. F. Moult, "Spectroscopic and laser characteristics of Ti:Al_2O_3", J. Opt. Soc. Am. B **3**, 125-133 (1986).

[19] A. V. Sokolov, D. R. Walker, D. D. Yavuz, G. Y. Yin, and S. E. Harris, "Raman generation by phased and antiphased molecular states", Phy. Rev. Lett. **85** , 562-565 (2000)

[20] J. Q. Liang, M. Katsuragawa, F. Le Kien, and K. Hakuta, "Sideband generation using strongly driven Raman coherence in solid hydrogen", Phys. Rev. Lett. **85**, 2474-2477 (2000)

[21] T. Suzuki, M. Hirai, and M. Katsuragawa, "Octave-spanning Raman comb with carrier envelope offset control", Phys. Rev. Lett. **101**, 243602 (2008)

[22] S. Zaitsu and T. Imasaka, "Continuous-wave anti-Stokes Raman laser based on phase-matched nondegenerate four-wave mixing", Opt. Lett. **40**, 73-76 (2015)

[23] E.R. Brown, K. A. Mcintosh, K. B. Nicols, and C. L. Dennis, "Photomixing up tp 3.8 THz in low-temperature-grown GaAS", Appl. Phys. Lett. **66**, 285-287 (1995)

[24] D. D. Yavuz and J. J. Weber, "Tunable source of terahertz radiation using molecular modulation", Opt. Lett. **37**, 4191-4193 (2012)

[25] V. Menoret, R. Geiger, G. Stern, N. Zahzam, B. Battelier, A. Bresson, A. Landragin, and P. Bouyer, "Dual-wavelength laser source for onboard atom interferometry", Opt. Lett. **36**, 4128-4130 (2011).

[26] R. M. Measures, Laser Remote Chemical Analysis (Wiley, 1988).

[27] W. L. Eberhard and R. M. Schotland, "Dual-frequency Doppler-lidar method of wind measurement", Appl. Opt. **19**, 2967-2976 (1980).

[28] R. Diaz, S. C. Chan, and J. M. Liu, "Lidar detection using a dual-frequency source", Opt. Lett. **31**, 3600-3602 (2006).

CHAPTER 2

Dual-Frequency Laser System

2.1 Introduction

The goal of this work is to develop a dual-frequency laser with an excellent performance in terms of the power, beam quality, power stability, frequency selectivity and relative output power controllability. This chapter describes the main components of the dual frequency injection-locked laser system that can fulfill the goal of this research work. There are a few choices to realize the stable dual-frequency injection locked laser, here we select a method in which the seed frequencies are locked to a high finesse cavity and introduced into the power oscillator. Later, power oscillator is locked at simultaneous dual-frequency resonance. In order to realize the simultaneous resonance of the two frequencies with the power oscillator, we insert a pair of wedge plates in the optical path of the power oscillator cavity. Although this method is a bit complex compared to the other possible methods such as locking the frequency directly to the power oscillator cavity [1]. It has advantages in terms of laser linewidth, which depends on the locking cavity finesse, in this case it is the master cavity finesse. In the later case, it is limited by the power oscillator cavity finesse, which should not

be increased to a high value.

2.2 Injection-locking and locking range

Injecting a weak laser frequency into a high power free-running oscillator can produce a high power laser with the similar features of the injected weak signal [2]. Consider a single frequency laser operating at a frequency ω_0 with a free running output power P_0. Consider a ring cavity and a weak seed frequency ω_1 with a power P_1 is incident on the cavity output coupler. Depending on the power and frequency of the incident weak signal will amplify in the power oscillator. As shown in figure 2.1, the maximum power produced at ω_0, but there exists small gain at ω_1.The regenerative gain for the electric field of a weak beam reflecting from the output coupler can be written as

$$g(\omega_1) = \frac{r_1^2 - G(\omega_1)}{r_1(1 - G(\omega_1))} \tag{2.1}$$

where r_1 is the output coupler reflection coefficient and $G(\omega_1)$ represents the round trip gain at ω_1. The round trip gain can be written as $G(\omega_1) = (r_{eff})e^{(-\alpha_0 l_0)}e^{(\alpha_{eff} l_{eff})}$ $e^{-i(\omega_0-\omega_1)L/c}$ Here r_{eff} is the reflection coefficients of the cavity mirrors except for the output coupler, $e^{(-\alpha_0 l_0)}$ represents the absorption losses of the cavity, $e^{(\alpha_{eff} l_{eff})}$ represents the gain in the cavity, c is the velocity of the light and L is the cavity round trip optical path length. Under the assumption of the $\omega_1 \sim \omega_0$, the equation 2.1 can be written as

$$g(\omega_1) = \frac{(1 - r^2)c/L}{i(\omega_0 - \omega_1)} \tag{2.2}$$

As shown in the figure 2.1, as the seed frequency approaches the ω_0, the seed amplified rapidly inside the power oscillator cavity, which is represented by the solid red curve. When the seed frequency ω_1 is sufficiently close to the free-running frequency ω_0, the free running power at ω_0 is suppressed a lot and the most of the power oscillates at the injected frequency ω_1. This will happen from either side of the center frequency. The points at which the injected signal oscillates with the maximum power or the free-running power vanishes fully are called the locking points, which are represented

by A, B. The frequency spacing between these two points are called the full locking range. The locking range can be defined by the following equation,

$$\Delta\omega_{lock} = 2(1 - r^2)\frac{c}{L}\sqrt{\frac{P_{master}}{P_{freerun}}} \tag{2.3}$$

According to this equation, the locking range depends on the ratio of the master and free-running powers. Also it is understandable, to a fixed locking range, as the free-running power increases, more seed power will be required. If we want to drive a high power oscillator, it is necessary to inject more seed power, which is difficult in the most of the cases.

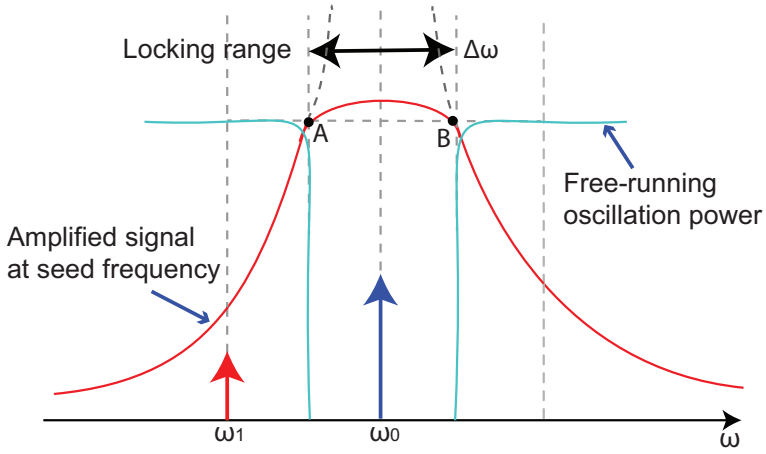

Figure 2.1: Illustration of the injection locking range; A modified version of the A. E. Siegman, Lasers (1986)

2.3 DFIL laser system

The DFIL laser system can be mainly divided into three parts. 1. Master cavity, 2. Seed lasers system, and 3. Power oscillator

2.3.1 Master cavity

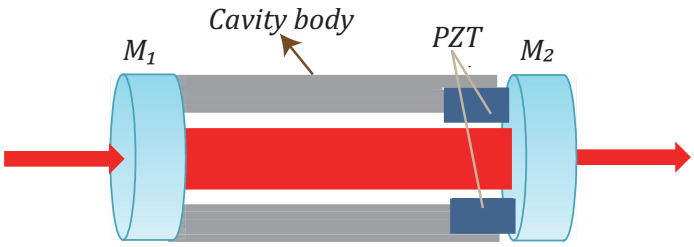

Figure 2.2: Illustration of the master cavity. M1 and M2 are highly reflective cavity mirros; PZT, piezoelectric transducer.

The master cavity is a high finesse optical cavity with an optical finesse of 6,500 and cavity length 6cm. The corresponding free spectral range is 2.5 GHz and the allowed linewidth (Full width at half maximum) of the cavity is 1.3 MHz. This cavity is designed in the semi-confocal configuration with a flat mirror ($R = \infty$) and a concave mirror ($R = 200\ mm$) as shown in the fig.2.2. Both the mirrors are highly reflective over the wavelength range $700 - 900\ nm$. The beam waist diameters at the flat and curved mirrors are $\sim 300\mu$m and 400μm respectively. As shown in figure 2.2, one of the mirrors is fixed to a rigid hollow cylindrical body. The cavity body is made of ultra low thermal expansion glass material to reduce the thermal fluctuations. The PZT (Piezo electric-transducer) is fixed properly to the rigid body by utilizing the drill inside the body. The remaining mirror is fixed to the rigid body through a PZT to adjust and modulate the cavity length. The PZT has a groove with hole diameter of 4mm, which is sufficiently greater than the mode profile at the mirrors. The same master cavity can be used as a enhancement cavity to check the nonlinear optical phenomenon of a gas medium. For this purpose this cavity is kept inside a chamber

which can be filled with a gas medium depending on the application.

2.3.2 Seed lasers system

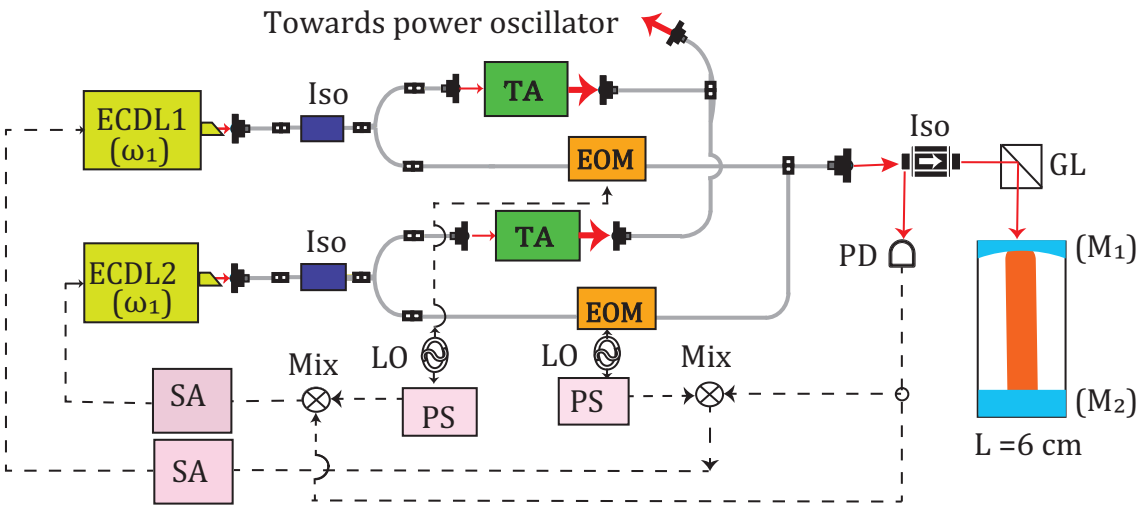

Figure 2.3: Illustration of the seed lasers system. ECDL, external-cavity controlled diode laser; Iso, inline isolator; TA, tapered amplifier; EOM, electro-optic modulator; PD, photo-detector; GL, glan laser polarizer; PS, phase shifter; LO; local oscillator; Mix, radio frequency mixer; SA, servo amplifier

Our seed lasers are home made external cavity diode lasers (ECDLs). Each ECDL can deliver 20-30 mW output power at 100 mA operating currents (laser diodes purchased from Eagleyard photonics). These ECDLs can be continuously tunable up to a few GHz, using a PZT on which the grating was mounted.The diodes output frequencies can be select with in the gain width of few 10s of nm. The estimated free running frequency fluctuations are on the order of 1MHz. These ECDLs frequencies are stabilized to the master cavity by using well known Pound-Drever-Hall (PDH) frequency locking technique [3]. For this purpose, small fractions of the ECDLs powers are phase modulated by using the Electro Optic Modulators (fiber based) with different modulation frequencies (20 MHz and 32 MHz) and coupled to the master cavity as shown in figure 2.3. The reflected lights from the master cavity are detected by a single photo-detector (PD1). The PD1 signal split into two parts by

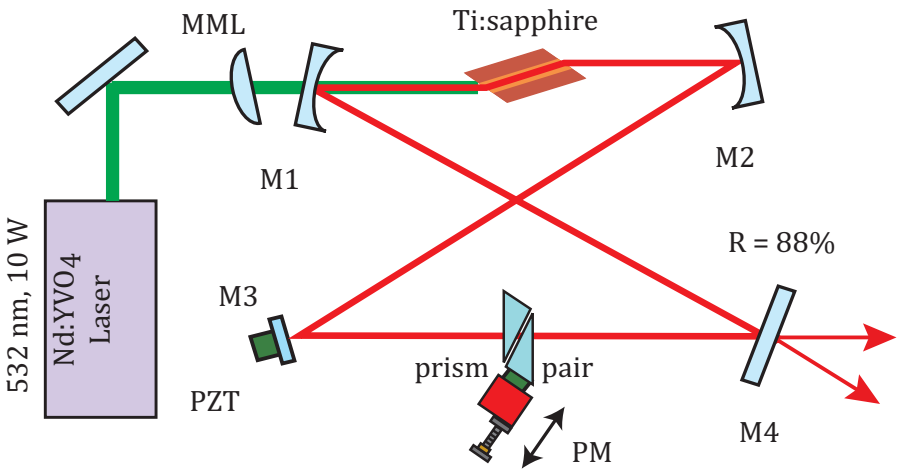

Figure 2.4: Illustration of the Ti:sapphire power oscillator. MML, mode matching lens; M, mirror; PZT, piezoelectric transducer; R, reflectivity; PM, pico motor.

using a power divider and mix with the reference frequencies (20 MHZ and 32 MHz) from the function generators and generate two independent error signals. These error signals are feedbacked to ECDLs current controllers through servo amplifiers (Vincent Photonics) to stabilize the frequencies. The stabilized frequencies are sent to corresponding tapered amplifiers and amplified up to ∼100 mW each. These amplified seed powers are mixed inside a fiber and coupled to the power oscillator cavity using a suitable mode matching lens.The detailed system of the seed lasers is shown in figure 2.3.

2.3.3 Power oscillator

The power oscillator was constructed in a bow tie ring cavity (round trip length 480mm, FSR 625 MHz) with a combination of four mirrors (two are flat and two are curved), a gain medium and a pair of transparent wedges as illustrated in figure 2.4. The gain medium was a Brewster cut Ti: Sapphire crystal of length 20 mm (0.25 % Ti^{3+} doped), mounted on a water cooled copper heat sink and fixed on a rotational stage to adjust the crystal angle with respect to the incident beam. The

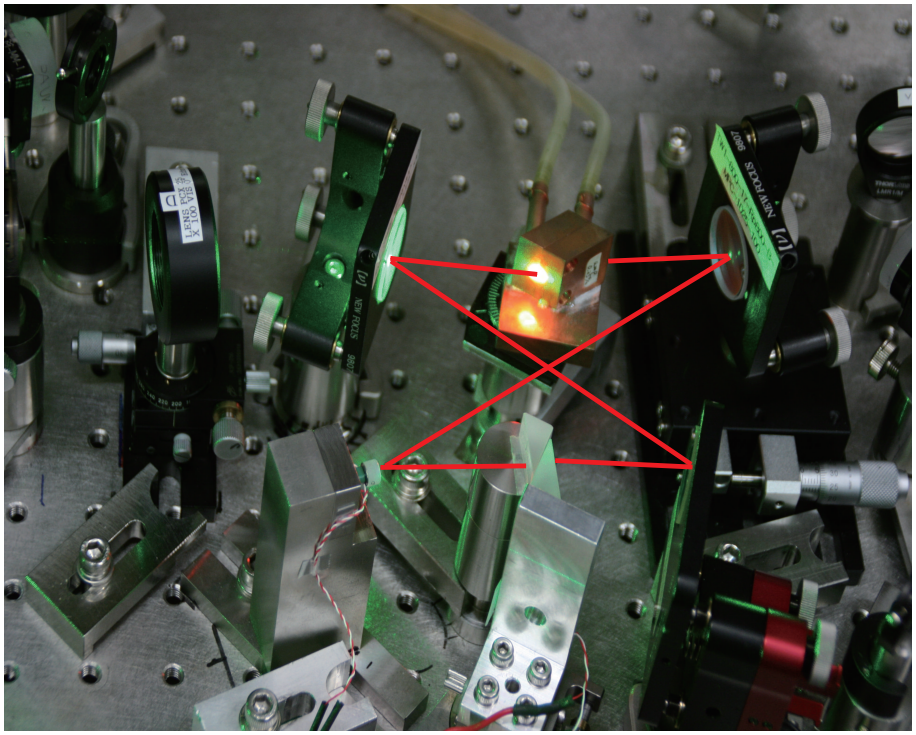

Figure 2.5: Photograph of Ti: sapphire bow-tie ring cavity power oscillator

whole component is placed between the two curved mirrors M1 and M2 (radii of curvatures 100mm each) as shown in the photograph (figure 2.5). The mirror M2 was mounted on a translation stage to adjust the distance between the two curved mirrors, which is crucial to obtaining good spatial beam profile and also it is sensitive to lasing. One of the flat mirrors M3 was mounted on a piezoelectric transducer (PZT) to adjust and modulate the cavity length. The resonance frequency of the PZT along with the mirror is an important parameter to obtain stable locking. Due to this reason we select the PZT (AE0203D04F, NEC/Tokin) and mirror (mass$\sim 0.31g$) for a high resonance frequency of $\sim 200kHz$. The remaining flat mirror M4 serves as an output coupler with a reflectivity 88% at both of the seed wavelengths, whereas all other mirrors have high reflectivity ($\sim$99%) at these wavelengths. The pair of transparent wedges were positioned between the two flat mirrors to adjust the optical length of the power oscillator cavity (few nm to few mm range) without disturbing the cavity confinement. Both the wedges have anti-reflection coatings (reflectivities $<$0.25%) to reduce the internal losses of power oscillator cavity. The power oscillator

was pumped by a 10W frequency doubled Nd: YVO4 laser (Coherent, Verdi-10). The 532 nm pump laser is introduced into the power oscillator cavity through the curved mirror M1 with the help of a mode matching lens (MML f=100mm). The MML is tilted slightly to obtain optimal spatial overlap between the pump laser and the bow tie cavity spatial modes. The digital photo graph of the power oscillator cavity is shown in figure 2.5, in which the mounting of optics, Ti: sapphire crystal and wedge pair are shown clearly.

The total (DFIL) laser experimental system including with stabilization electronic feedback loops are shown in figure 2.6. To stabilize the power oscillator cavity for simultaneous two frequency oscillation, a small leakage power from the mirror M2 is taken and split into the individual frequencies with the help of an optical grating element. These separated frequencies were detected by the photo detectors PD2 and PD3. A part of these detected signals are used for feedback and remaining part of these signals were used for monitoring.The power oscillator cavity PZT is set to the 17 kHz sinusoidal modulation around the simultaneous two frequency resonance position and the cavity length is locked to the one of these seed frequencies by feedback the error signal to the PZT.

The output of the DFIL laser can be coupled to the master cavity depending on the application. The dotted red line in figure 2.6 represents the optical path to couple the DFIL laser to the high finesse cavity. With this technique, it is easy to couple the multiple frequency beam to a high finesse cavity where the seed frequencies are stabilized to the same high finesse cavity.

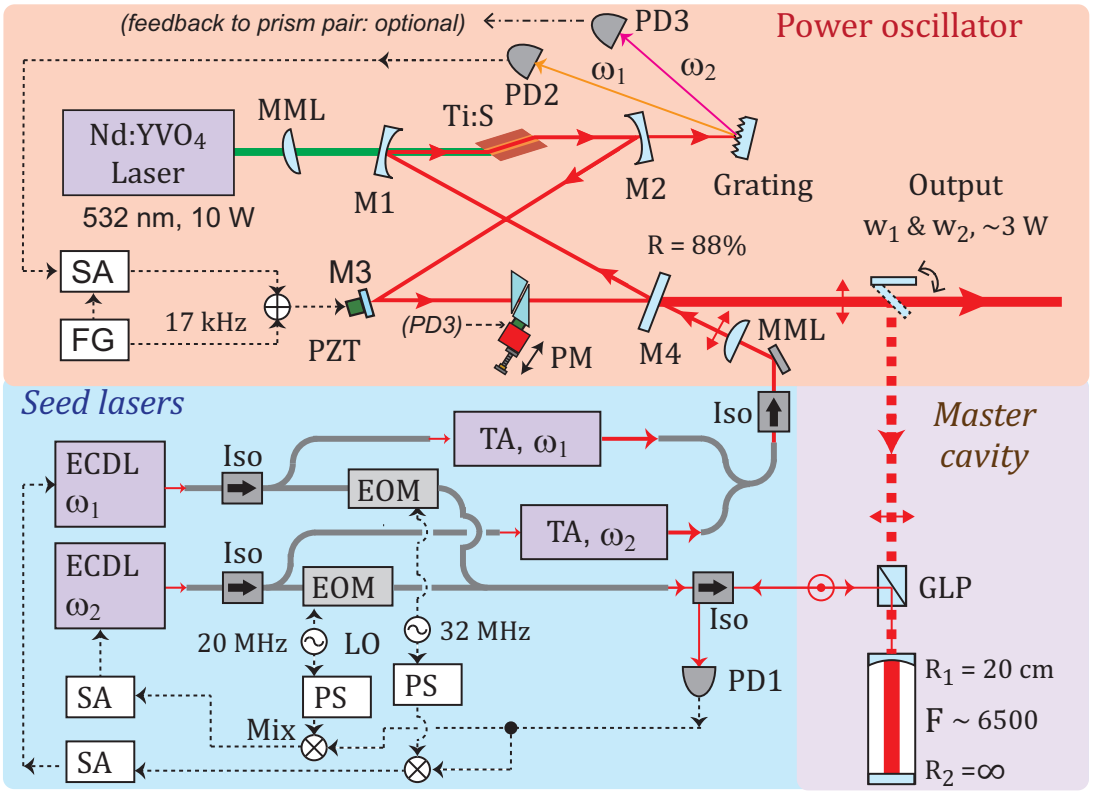

Figure 2.6: Illustration of DFIL Ti:sapphire laser total experimental system. PD2 and PD3, photo-detector; SA, servo-amplifier; FG, function generator; GLP; Glan laser polarizer

2.4 Conclusions

In this chapter we have proposed a method to realize the dual-frequency laser from single laser cavity. The overall dual-frequency laser system has shown and also presented the importance of the each element. The operational procedure of the DFIL laser and its characteristics will be discussed in the following chapter.

Bibliography

[1] E. A. Cummings, M. S. Hicken, and S. D. Bergeson, "Demonstration of a 1-W injection-locked continuous-wave titanium:sapphire laser", Appl. Opt. **41**, 7583-7587 (2002).

[2] A. E. Siegman, "Lasers, University science books", (1986).

[3] R. W. P. Drever, J.L. Hall, F. V. Kowalski, J. F. Hough, G. M.Ford, A. J. Munley, and H. Ward, "Laser phase and frequency stabilization using an optical resonator", Appl. Phys. B **31**, 97-105 (1983).

CHAPTER 3

Dual-frequency laser characteristics

3.1 Introduction

In the previous chapter, the dual-frequency laser system and its components were illustrated. In this chapter, the laser fundamental characteristics such as spectral purity, spatial mode profile, output power stability and as the advanced features arbitrary two frequency selection and controllable relative output powers are presented.

3.2 Seed frequencies stabilization

Stable seed frequencies are necessary to obtain stable dual frequency laser oscillation through the injection locking technique. The ECDLs frequencies were stabilized to a high finesse (6,500) reference cavity by using the PDH locking technique [1]. For this purpose, the seed frequencies ω_1 and ω_2 were modulated using inline fiber EOMs. In this case the reflected lights from reference cavity were detected with a single photo detector. Different modulation frequencies (20MHz and 32 MHz) were applied to distinguish the error signals. These modulation frequencies were sufficiently large

and well outside the cavity allowed line width of 400 kHz, which was estimated from the cavity FSR 2.5 GHz and finesse 6,500. The stabilized laser line widths were much smaller than this cavity allowed line widths. The black curves in figure3.1a and 3.1b are the error signals corresponding to the seed frequencies ω_1 (784nm) and ω_2 (806nm), which were recorded by sweeping the seed laser frequencies around the cavity resonance. The seed lasers frequencies were locked to the reference cavity using the PDH locking technique and the stabilized error signals were shown in red curves. These stabilized error signals were well suppressed under the locking state.The frequency stabilities were estimated to be 40 kHz rms value under the locking condition and it is possible to decrease the linewidth to a lower values by increasing the finesse of the locking cavity and by preparing stable cavity length [2].

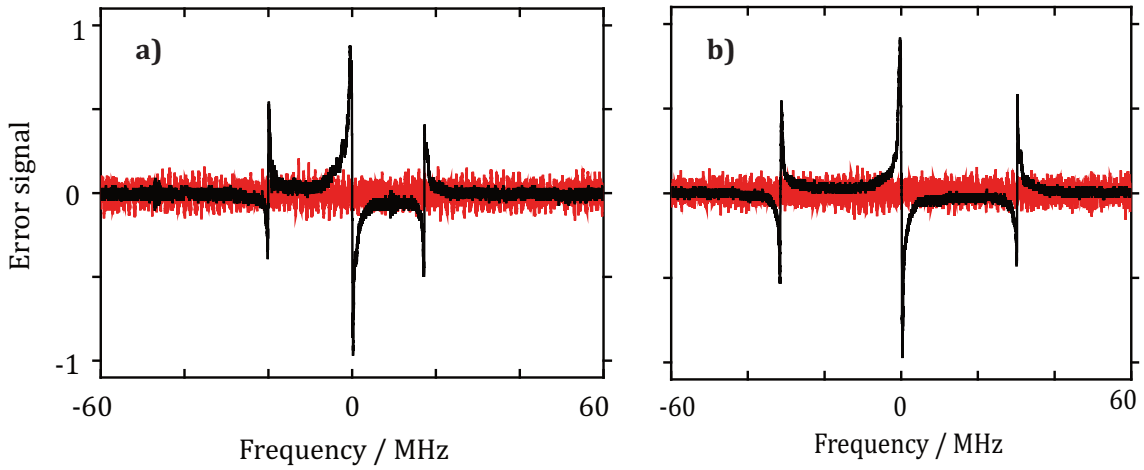

Figure 3.1: (a) and (b) are the PDH error signals corresponding to the frequencies ω_1 and ω_2. The black curves are the error signals while sweeping the frequency around the cavity resonance and the red curves are the error signals after the frequency stabilization

3.3 Stabilization of power oscillator for simultaneous two frequency resonance

The frequency stabilized seed lasers were injected through output coupler by using a suitable mode matching lens. At first, we checked the seed frequencies (ω_1 and ω_2) resonances with power oscillator cavity. For this purpose, Small leakage power through the mirror M2 split into the individual frequencies with the help of an optical grating element. These separated frequencies were detected by the photo detectors PD2 and PD3. A part of these detected signals were used for feedback and remaining part of these signals were used for monitoring. The bow tie ring cavity was modulated with a 10 Hz frequency and the recorded longitudinal mode profiles of the the seed frequencies ω_1 and ω_2 were shown in figure 3.2, black and red curves. From these mode profiles the cavity finesse of the bow tie ring cavity power oscillator was estimated to be 35, this value was close to the finesse of 37, which was derived from the output coupler 88%, and round trip losses in the power oscillator cavity, 4%. Now by monitoring these modes, the optical cavity length was adjusted to get simultaneously two frequency resonance with the help of the the prism, which was mounted on a pico-motor translational stage. The overlapped longitudinal modes of the power oscillator corresponding to the seed frequencies are as shown in figure 3.2 (black and red Lorentzian curves). The cavity PZT was set to the 17 kHz sinusoidal modulation around the simultaneous two frequency resonance position and the cavity length was locked to the one of these seed frequencies by fed back the PD signal to the PZT. For the stabilized power oscillator cavity, the two seed frequencies transmissions were maintained at their maximums, as shown in figure 3.2 (black and red curves).

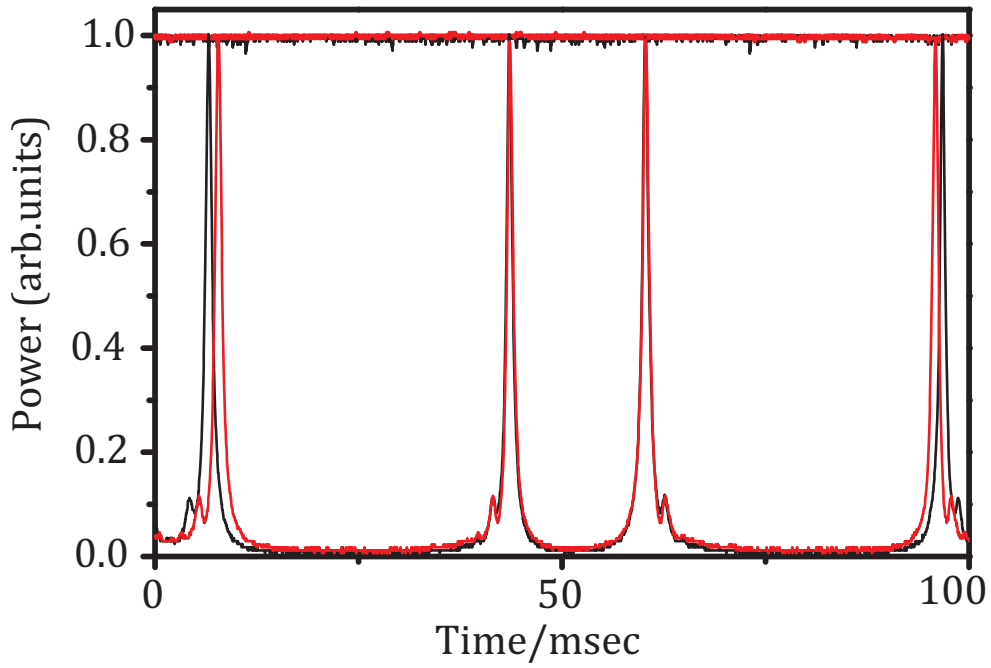

Figure 3.2: Simultaneous stabilization of the seed frequencies to the power oscillator cavity. Black and red Lorentzian curves are the longitudinal modes of the power oscillator cavity corresponds to the frequencies ω_1 and ω_2.

In this system the two frequency longitudinal mode overlap was crucial to obtain simultaneous two frequency resonance. Depending on the selected frequency pair the insertion length of the prism varies from few 10s of micro-meters to few millimeters. In the case of 784 nm and 806 nm frequency pair, the cavity length was tuned by 20 FSRs approximately, when the longitudinal mode overlap was at its maximum value. Which means the minimum required change in the optical length of the cavity is close to 16 μm. To obtain perfect overlap between the longitudinal modes, we need to repeat this process several times, this requires few 100s of μm. But, the selected frequencies are much closer than the above mentioned frequency pair, the required change in the optical length will be much greater than the above mentioned values. The required thickness to obtain the simultaneous two frequency resonance for various frequency pairs is shown in appendix A.

3.4 Simultaneous two frequency laser oscillation

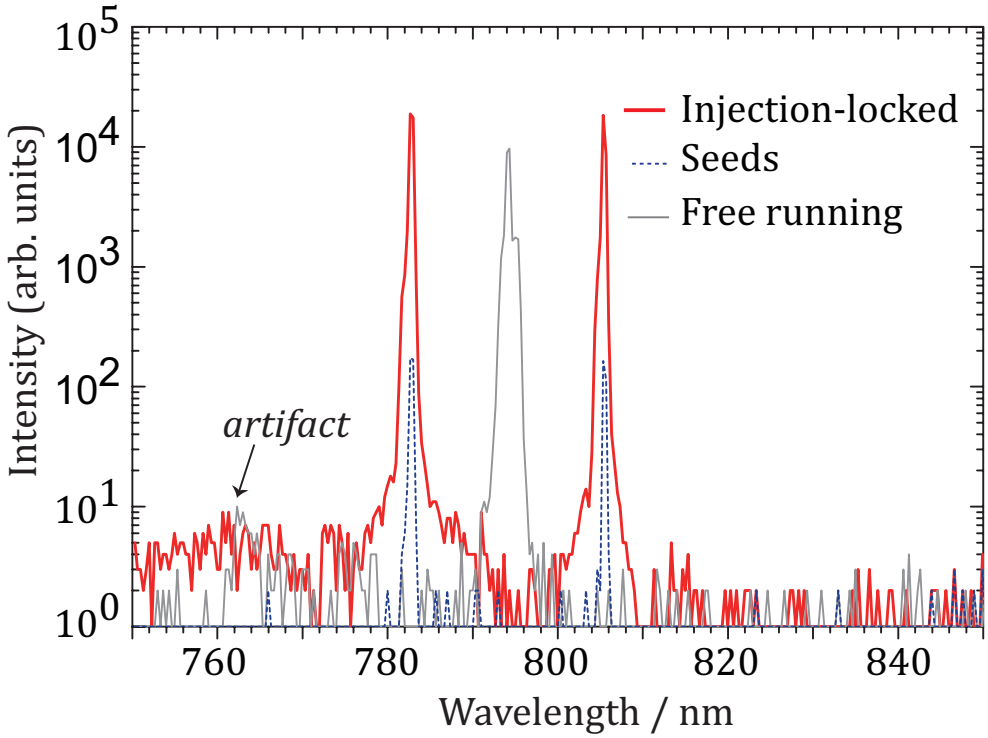

Figure 3.3: Dual-frequency injection-locked oscillation. The red curves are the injection locked simultaneous dual-frequency oscillation, the gray curve is the free running oscillation and the dotted blue curves represent the seed frequencies.

After realized the seed frequencies resonances with the power oscillator cavity, the pump power of a maximum of 10 W was introduced into the power oscillator cavity. Repeated the above mentioned process and obtained simultaneous two frequency oscillation. The output spectrum of the injection locked dual frequency laser was recorded with the optical multi-channel analyzer (OMA; Andor DU420-OE) and is shown in figure 3.3. The red curves in the figure represent simultaneous dual-frequency injection locked state, the gray curve at 795 nm represents the free-running oscillation and the dotted blue curves represent the seed frequencies that were injected into the power oscillator. The dual frequency laser oscillations were coincide with the injected seed frequencies. Under injection locking the free-run has suppressed greatly

as shown in the figure (by > 30 dB). Even though in the spectrum the free-running and the injection locked oscillations had similar line widths, it was because, the OMA resolution was not sufficient in this case. In reality, injection locked frequencies have narrow line widths compared to the free-running oscillation, which will be discussed in the later sections. The higher noise level around 760 nm corresponds to the instrumental artifact, not because of the spectral broadening or any other frequency oscillations.

3.4.1 Free run suppression and power spectrum

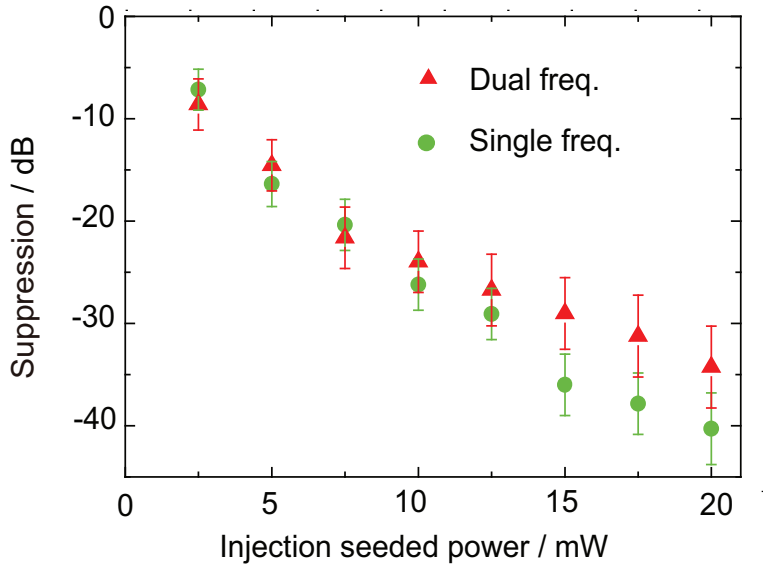

Figure 3.4: Free-running suppression as a function of total injection seeded power. The green circles and red triangles are the free-running suppression in the cases of single and dual-frequency injection locking states respectively.

To know the minimum seed-power required for DFIL laser operation, we studied the free-running suppression as a function of the total injected seed powers in the case of dual-frequency injection locking as well as single-frequency injection locking state.The results were shown in figure 3.4. The red triangles represented the free-running suppression of the dual-frequency injection locked state and the red circles represented

the free-running suppression of the single-frequency injection locked states.This suppression behavior of the two frequencies was similar to that with a single-frequency injection-locked oscillation. From the figure, it has shown that 20 mW seed powers were sufficient to suppress the free-running oscillations below to 30dB. Obtaining such low seed powers are easy and one can get it from diode lasers without any external power amplifiers. The seed power required for stable DFIL oscillation can also be derived by estimating the locking range [3], yielding a result of 10μW for a seed linewidth of 40 kHz. As observed here, in reality 20 mW was required to have sufficient suppression of 30 dB, which is much larger than the above estimation. One of the main factor that effects the required seed powers is the spatial overlap of the seed mode profile and pump mode profile along with the cavity mode profile.

At the optimum cavity alignment, we measured the output powers as a function of the pump powers and the results are as shown in figure 3. 5. The black squares represent the total output power of the free-running oscillations. It was measured simultaneously at the two outputs of the ring cavity by using two power meters. The red circles represent the total output power of the injection locked dual-frequency oscillation case. The lasing threshold was 2.0 W and the maximum obtained output power was 2.8 W at 10 W pumping power, which was similar to that of the total free-running power. The slope and energy-conversion efficiencies were 35% and 28%, respectively. These specifications were nearly the same as those in single-frequency operation. The blue and the light gray triangles represent the injection locked output powers corresponding to the frequencies 784nm and 806 nm under similar injected seed powers and these are measured by separating the frequencies using a dispersive prism.

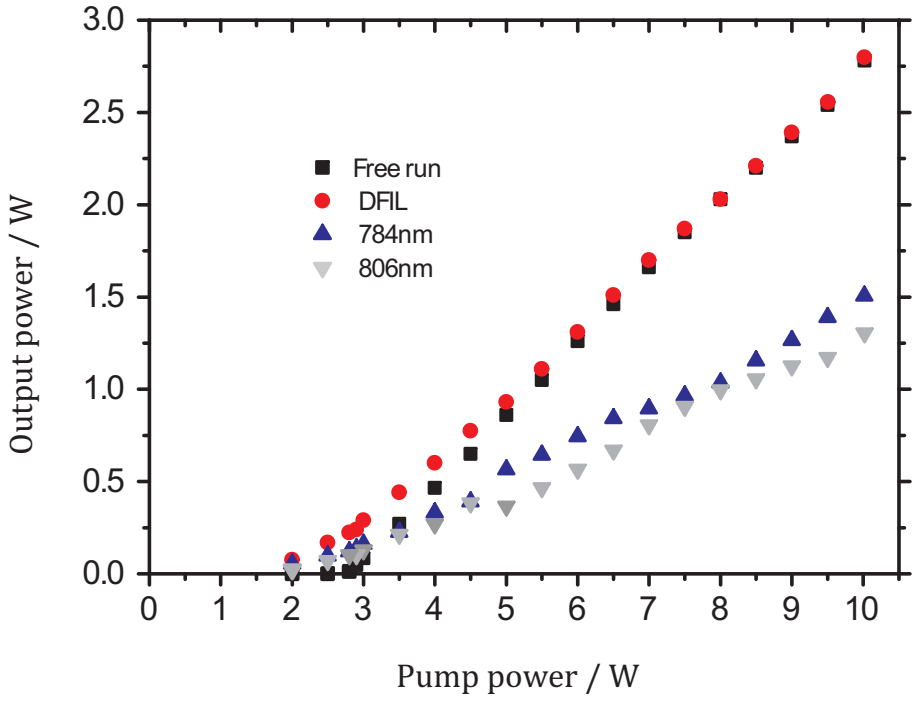

Figure 3.5: Dual frequency output power as a function of the pump power. The black squares and the red circles are the total output powers in the case of free running and injection locked states respectively.

3.5 Fundamental features of the DFIL laser

The applications of a laser system mainly depends on its basic parameters such as spectral purity, spatial beam profile and power stability. Here, we analyze these basic features of the dual-frequency injection-locked laser, which will influence the quality of the data in many optical science experiments.

3.5.1 Spectral purity

In order to check the spectral purity, a small fraction of the laser output power was coupled to a optical spectrum analyzer (FSR: 2 GHz and finesse:100). The results were shown in figure 3.6. The two longitudinal modes (red), corresponding to the two seed frequencies, ω_1 and ω_2 , were clearly confirmed with an instrumental resolution

of 20 MHz; no other modes were seen. Where as in the free-running case, the laser oscillated in the multiple longitudinal modes as shown in the figure (gray curves). We further evaluated spectral purity by creating a beat between the injection locked laser output and seed frequency, where the seed frequency was shifted by 110 MHz with an acoustic optical modulator and the results were shown in figure 3.7. The curve with blue squares represent the RF beat spectrum of the seed frequency to the frequency shifted seed frequency. The curve in the red circles represent the RF beat spectrum corresponding to frequency shifted seed laser frequency and the injection locked Ti:sapphire laser output frequency. Both the beat spectra have similar widths and no apparent spectral broadening from the seed line-width was observed at a 1 kHz frequency resolution of the RF spectrum analyzer.

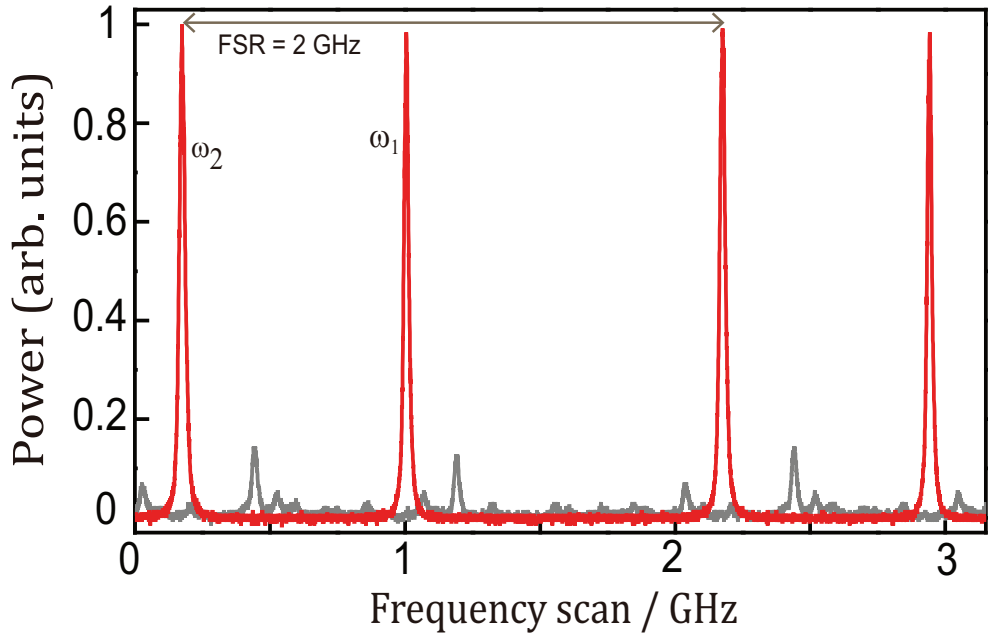

Figure 3.6: Longitudinal mode analysis with a Fabry-Perot spectrum analyzer. The red and the gray curves are the longitudinal modes in the case of injection locked and free-running states respectively.

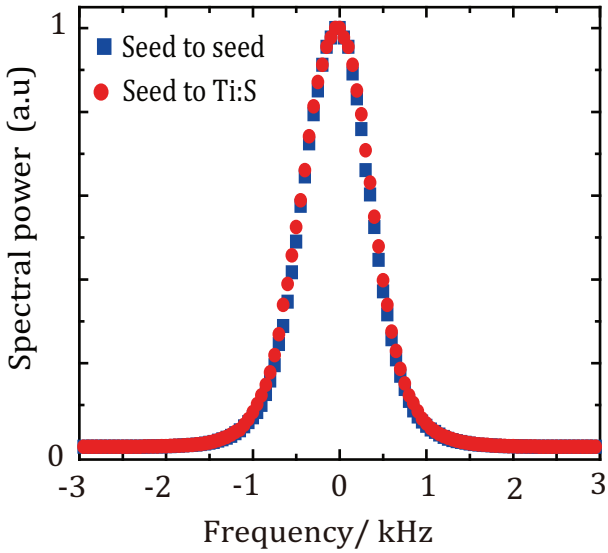

Figure 3.7: Beat note between the injection locked output frequency and the frequency shifted seed frequency

3.5.2 Spatial mode purity (M^2 measurement)

Another important parameter of a laser is the spatial mode purity. To check the spatial purity of the DFIL laser, we measured the M^2 parameter. The results were shown in figure 3.8. In this measurement, we selected either of the two frequency beams by using a band-pass filter and measured the beam profiles with the CCD camera as a function of distance from the beam waist position. The solid red circles and the solid black triangles represent the beam diameters in the X-direction and the open circles and open triangles represents the beam diameters in the Y-direction. The solid and dashed curves represent the fitted experimental data. For both the frequencies the measured M^2 factors were close to unity. Although a small astigmatism was included mainly because of the bow-tie ring cavity configuration but it can be compensated simply by using an appropriate cylindrical-lens pair, if required in an application. The inset figure 3.8 shows the photo graphs of the injection locked laser outputs, the left side figure represents the combined two frequency output beam, with clear mode profile. It also tells us the good spatial overlap of the two frequency beams. Which is

one of the important feature of the dual frequency injection locked laser. This kind of spatially overlapped multiple frequency beams are useful in the study of the nonlinear optical phenomena, where the spatial overlap of the frequency beams plays a crucial role. In this case the output of the DFIL laser was able to couple to the single mode fiber with a coupling efficiency more than 80%, which was confirmed the good spatial mode profile of the injection locked laser. The right side of the inset figure represents the digital photograph of the DFIL laser output after passing through a dispersive prism. It showed the clear beam profiles of the two frequency beams.

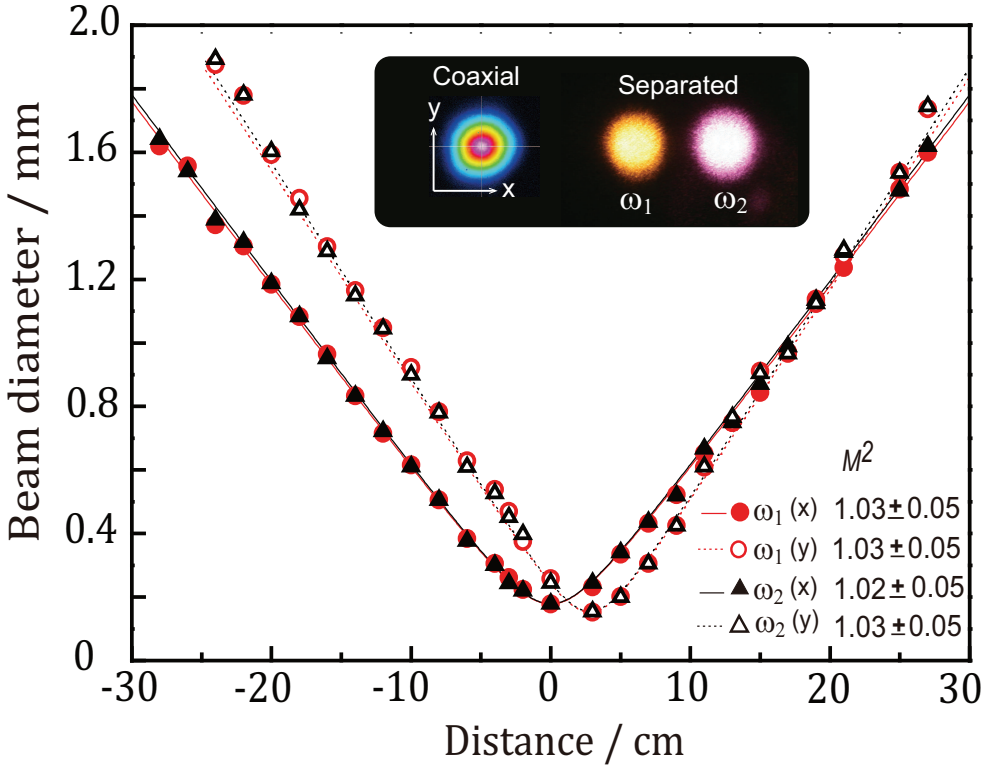

Figure 3.8: Analysis of spatial mode purity by M^2measurement. The red circles and black triangles represent the beam diameters corresponding to the frequencies ω_1 and ω_2 respectively

3.5.3 Output power stability

The power stability of a laser is an important parameter in the experiments. For this purpose, a small fraction of the output was separated into its individual frequencies using a grating element and detected by two independent photo-detectors. The results are shown in figure 3.9. The measured rms power fluctuations were 1% at ω_1 (red) and 2% at ω_2 (black) on a short time scale of 100 ms as shown in figure 3.9a. The power fluctuations were similar even over a long time scale of 450 s, i.e., 1% at ω_1 and 2% at ω_2 as shown in the figure 3.9b . Here, we did not see any instability caused by nonlinear processes such as competition between the two frequencies. The slightly larger fluctuation at ω_2 was due to the mechanism, whereby the power oscillator was locked to the master reference cavity by the ω_1 seed only. The power oscillator cavity was not stabilized for the second frequency. In this case, the long time stability some times interrupted by the reference cavity thermal fluctuations, to which the seed frequencies were stabilized. The ECDL frequencies followed the reference cavity and the power oscillator followed the seed frequencies, this means the power oscillator followed the master cavity. The thermal drift in the cavity length causes the drift in the frequencies which disturbs the simultaneous dual frequency resonance state. This can be overcome by giving a second feedback to the power oscillator cavity, through the wedge which was fixed on the pico-motor stage.

Up to this point, we have described the fundamental characteristics of the DFIL laser such as, single longitudinal/transverse mode nature and practical power stability. These characteristics imply that the DFIL laser is applicable to a variety of purposes.

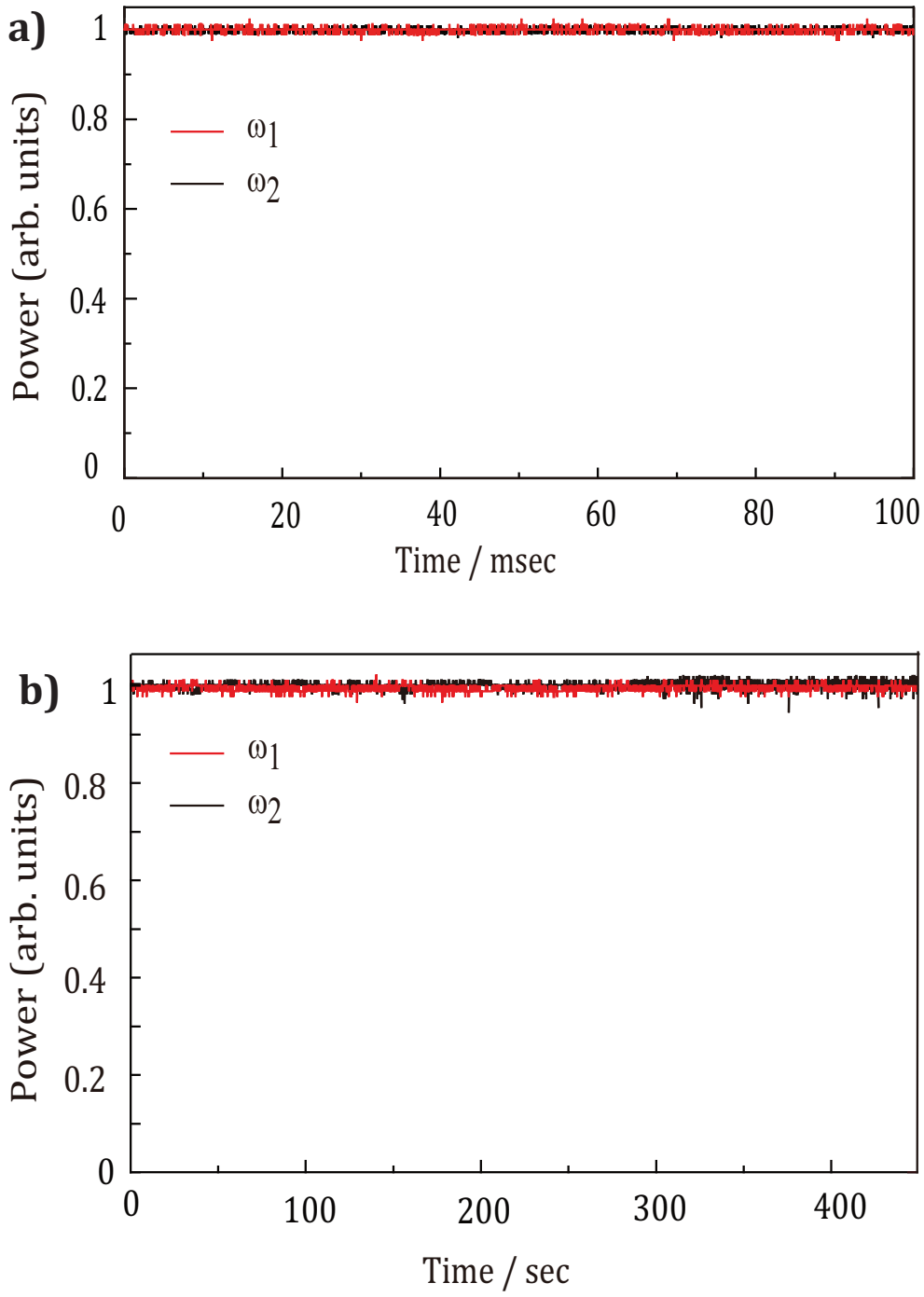

Figure 3.9: Output power stability of the DFIL laser a) short time duration power stability observation and b) relatively long time duration power stability observation

3.6 Advanced features of the DFIL laser

From the viewpoint of applications, especially when they include nonlinear optical processes, selectivity of the wavelength combinations and precise controllability of the output-power ratios at the two selected wavelengths will be key issues.Here, we demonstrate these advanced abilities in this DFIL laser system.

3.6.1 Arbitrary frequency separation

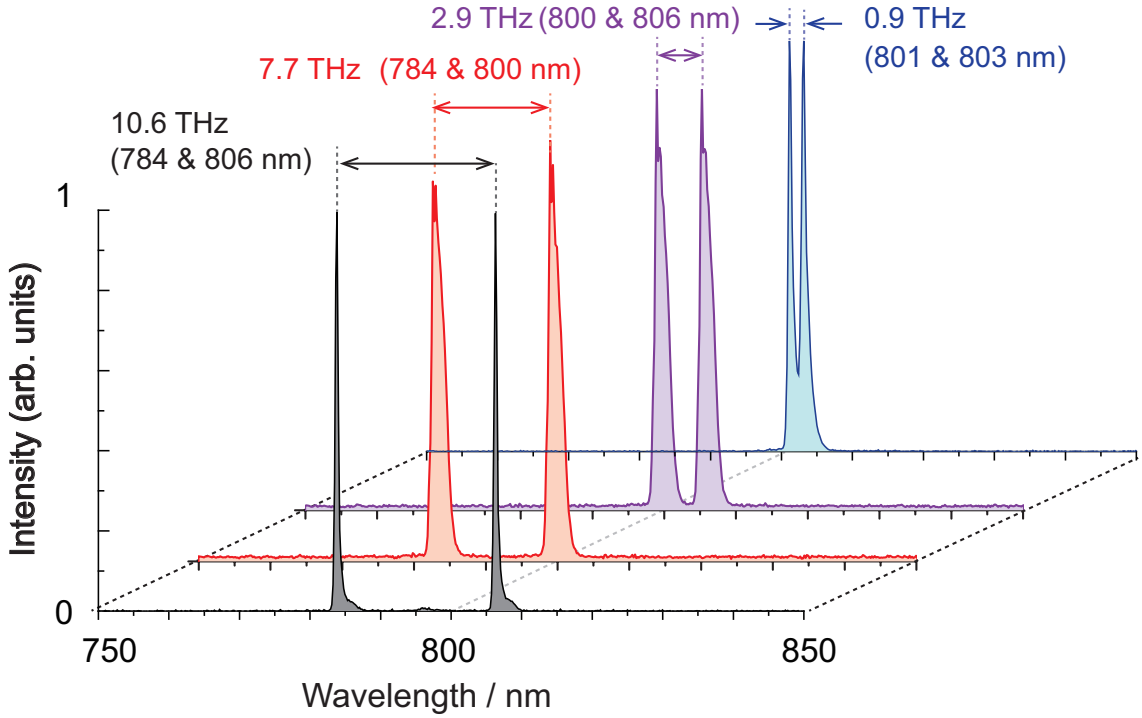

Figure 3.10: Arbitrarily separated frequency pairs.

Arbitrary separation of the frequency pairs is one of the advantages of the DFIL laser in the study of nonlinear optical processes. We tested various frequency combinations with frequency spacings from 500 GHz to 11 THz and several of them are shown in figure 3.10. The frequency spacings of the selected wavelengths were as follows: 10.623 THz (783.8849 nm, 806.2823 nm), 7.731 THz (783.8853 nm, 800.0595 nm), 2.895 THz (800.0590 nm, 806.2885 nm), and 0.867 THz (801.1395 nm, 803.0041 nm). For all of these wavelength pairs, we obtained stable DFIL oscillations with performances

equivalent to those reported in the previous sections. With this current system even larger frequency spacing is possible. If we exchange the output coupler and seed lasers appropriately, depending on the wavelength region, our DFIL laser can cover the entire gain region of a Ti:sapphire laser, from 670 nm to 1050 nm [4]. Note that the two frequencies can be selected continuously, although the power oscillator has a discrete modes, it is possible by controlling the insertion thickness of the wedges which were placed inside the power oscillator cavity. For any frequency combinations, whereas their frequency spacing must be greater than 100 GHz. Because in the current case the overlap of the arbitrary frequencies with a closer frequency spacing is limited by the allowed optical cavity length changes. In our current case we can change the optical cavity length to few mm to cm without disturbing the cavity confinement. For closer frequency spacings the current change is not sufficient. In the current case, we obtained a dual resonance condition by slightly adjusting the insertion thickness of the wedge pair into the power oscillator.

3.6.2 Relative power controllability

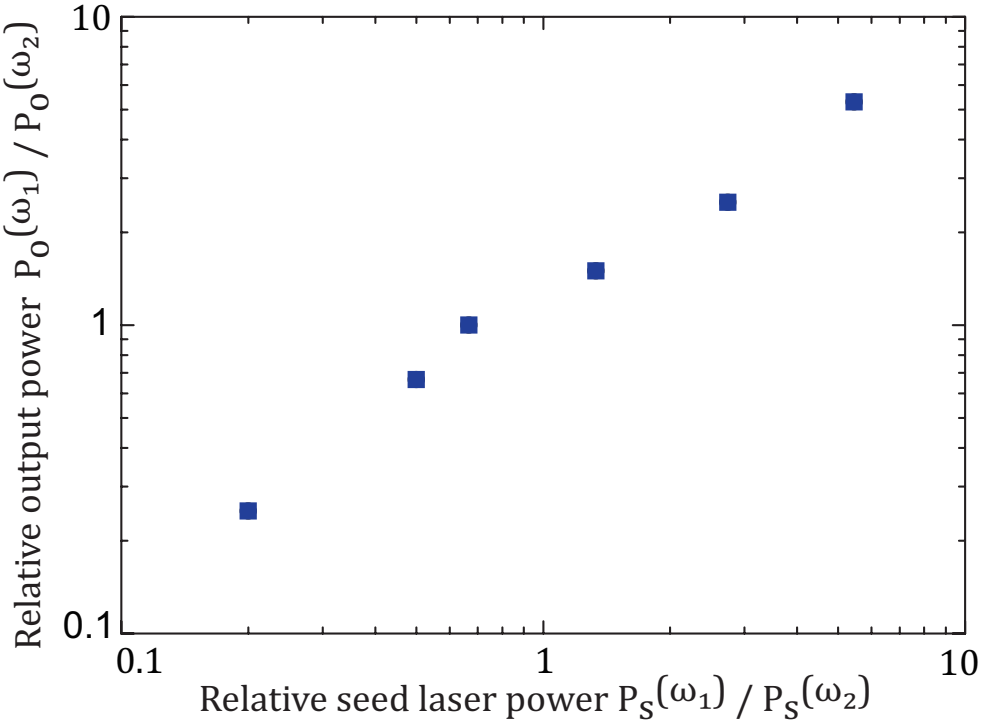

Figure 3.11: Controllable relative power ratios as the function of the injected seed powers

The relative power controllability of the output frequencies is an useful feature of the DFIL laser. Arbitrary control of the output-power ratio as a function of injected seed powers is shown in figure 3.11. In this case, the selected frequencies were 783.8849 nm (ω_1) and 806.2823 nm (ω_1). The output-power ratios at the two frequencies, ω_1 and ω_2 , can be flexibly controlled over a wide dynamic range of greater than 1 order by simply manipulating the seed-power ratios at the two frequencies. Some of the relative power ratios are shown in figure 3.11. At any power ratio, stable DFIL oscillations were observed with the same total output power, namely, 2.8 W; $(\omega_1/W; \omega_2/W)$ = (2.30, 0.47), (1.95, 0.84), (1.66, 1.12), (1.38, 1.40), (1.14, 1.62), (0.55, 2.24). in this case, we preserved total seed power at a constant to maintain good free-running suppression of $< 10^{-3}$. Note that the frequencies ω_1 (λ_1=783.8849nm)and ω_2 (λ_2 = 806.2823nm)

employed here provided a calculated gain-to-loss product ratio close to unity; this implies that the output power ratio varies almost linearly with the seed power ratio [5]. This expectation also was confirmed, as seen here. When we employed other frequency combinations, the output-power ratios followed different curves, whereas the controllabilities were the same. In the case of homogeneously broadening gain medium the total output power remains constant and it is shared between the two seed frequencies, it allows us to predict the power controllability. Which may not be possible to predict the out power in case of in-homogeneously broadened gain media.

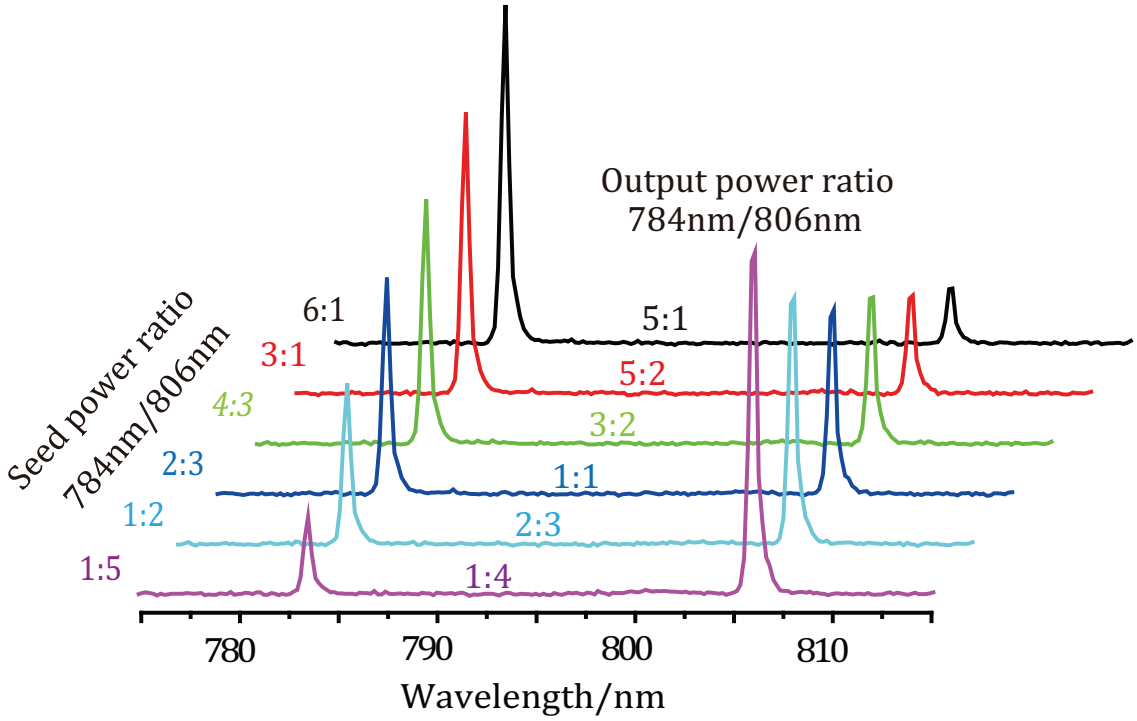

Figure 3.12: Arbitrary combinations of the output power

3.7 Conclusions

In this chapter, we have shown the realization of simultaneous two frequency oscillation from a single laser cavity. The DFIL laser basic features such as single frequency nature by using the scanning Fabry-Perot cavity and the single transverse mode pro-

file by measuring the M^2 factor were characterized. The DFIL laser practical power stability in short time scale and relatively long time scales were reported. DFIL laser free run power suppression as a function of injection seed power was discussed and also, compared with the single frequency injection locking case. Also, we have checked the output power as a function of pump power and obtained a maximum output power of 2.8 W. As the advanced features, desirable frequency separation of the two frequencies from 1THz to 10THz have realized with this injection locking technique. we have demonstrated the controllability of the relative output power ratios of the injected frequencies as a function of the injection seed powers.

The desired features of the dual frequency laser were realized with a good performance. Many of the optical science experiments needs the high frequency purity and good spatial mode profile, where these parameters effect the quality of the data, in such experiments it is very useful this kind of laser system. If we want to realize the two frequency mode overlap in free space from the lasers that are independently prepared is a difficult task. Also, it is difficult to combine the two or more closely separated frequencies with out the power loss. This DFIL laser system reduce the cost effect instead of using two laser systems, and makes it easy to deal with multiple frequencies. The relative power controllability is one of the best feature that will enhance the laser usage in the various optical science studies. If you compare with the other high power lasers such as master amplifier power oscillator (MOPA), DIFL laser has advantages such as high suppression of the spontaneous emission , good beam quality and well maintained polarization state.

Bibliography

[1] R. W. P. Drever, J. L. Hall, F. V. Kowalski, J. F. Hough, G. M. Ford, A. J. Munley, and H. Ward., "Laser phase and frequency stabilization using an optical resonator", Appl. Phys. B **31**, 97-105 (1983)

[2] D. G. Matei, T. Legero, S. Hafner, C. Grebing, R. Weyrich and W. Zhang, "1.5 μm lasers with sub 10 mHz linewidth", Phy. Rev. Lett. **118** (2017).

[3] A. E. Siegman, "Lasers", University science books, 1986

[4] P. F. Moult, "spectroscopic and laser characteristics of Ti:Al2O3", J. Opt. Soc. A **3**, 125-133 (1986).

[5] T. Onose and M. Katsuragawa, "Dual-wavelength injection-locked pulsed laser with highly predictable performance", Opt. Exp.**15**, 1600-1605 (2007).

CHAPTER 4

Study of Raman based molecular modulator

4.1 Introduction

As described and discussed in the previous chapter, the dual-frequency injection-locked laser has many advantages such as the mutual fine overlap between the two frequency beams, arbitrarily separated frequency pairs and controllable relative output powers. These features enhanced the laser applications in the various fields of optical science. In this chapter, one of the potential application of the dual-frequency injection-locked laser is described. The candidate is the Raman based molecular modulator using the para-H_2 gas as Raman medium, where strong two frequency laser field is essential to efficiently drive the molecular system.

Stimulated Raman scattering in the far of resonance case has been studied by using the femtosecond lasers in the impulsive regime [1] and by using the nanosecond lasers in the adiabatic regime [2–5]. Raman components in a wide frequency range spanning from IR to UV were generated using these techniques [6]. One of the advantage of these coherently generated frequency components is that to synthesis

ultra-short optical pulses in the time domain by coherent superposition of the optical fields. But the generation of broad band Raman components required high peak powers on the order of MW or GW/cm^2.

To reach such high peak powers with continuous wave lasers is a difficult task. But, the advantage of mirror coating technology is made this power levels possible with CW lasers by confining the laser frequencies to a high finesse optical cavity with a finesse greater than 10^5 or even more. In the CW regime using the high finesse cavities the first stokes laser was demonstrated by the Carlsten group [7], later the quantum limited anti stokes laser was generated by Imasaka group in 2008 [8]. Fetah Benabid et al., demonstrated the Raman generation in gas filled hollow core photonic crystal fibers [9].

4.2 Theory of Raman based molecular modulator

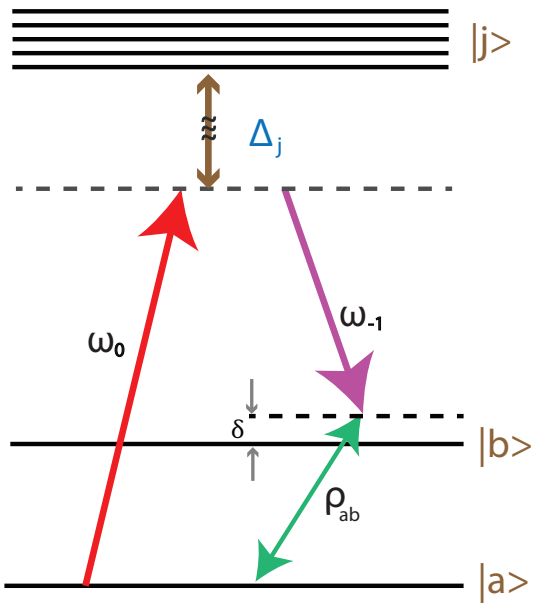

Figure 4.1: Energy level diagram of far-off resonant three level system driven by two strong laser fields.

Consider a three level Λ system as shown in the figure 4.1 . The solid horizontal lines represent the the energy levels of the molecule and the solid arrow lines represent the driving lasers ω_0, ω_{-1}. The states $|a\rangle$ and $|b\rangle$ are the ground and excited ro-vibrational states of the molecule respectively and the $|j\rangle$ represents the higher ro-vibrational and electronic states. The transition $|a\rangle$ to $|b\rangle$ is dipole forbidden and transitions $|a\rangle \leftrightarrow |j\rangle$ and $|b\rangle \leftrightarrow |j\rangle$ are far off single photon resonance. The upper gray dotted line represents the virtual state.

In the dipole approximation, the Hamiltonian of the system is given by

$$H = H_0 + H_{int} \tag{4.1}$$

where H_0 and H_{int} are expressed as

$$H_0 = \hbar\omega_a\sigma_{aa} + \hbar\omega_b\sigma_{bb} + \sum_j \hbar\omega_j\sigma_{jj} \tag{4.2}$$

$$H_{int} = -\sum_j E(\mu_{ja}\sigma_{ja} + \mu_{aj}\sigma_{aj} + \mu_{jb}\sigma_{jb} + \mu_{bj}\sigma_{bj}) \tag{4.3}$$

Here $\sigma_{\alpha\beta}$=$|\alpha\rangle\langle\beta|$ are the operators for level populations and transition amplitudes, E is the electric field, and μ_{ja} and μ_{jb} are the dipole moments of the transitions $j \leftrightarrow a$ and $j \leftrightarrow b$ respectively. We assume that the driving and generated fields propagate in the z direction where the local-time $\tau = t - z/c$. The total electric field is expressed in the form

$$E = \frac{1}{2}\sum_q (E_q e^{-i\omega_q\tau} + E_q^* e^{i\omega_q\tau}) \tag{4.4}$$

where ω_q can be expressed as follows

$$\omega_q = \omega_0 + (\omega_b - \omega_a - \delta) = \omega_0 + q\omega_m \tag{4.5}$$

here q is an integer number and ω_m is the modulation frequency. From the equation 4.5 the modulation frequency expressed as $\omega_m = (\omega_b - \omega_a - \delta)$ which is equivalent to the difference frequency of the applied fields ω_0 and ω_{-1}. The detuning δ is the difference

between the Raman transition frequency $(\omega_b - \omega_a)$ and the modulation frequency ω_m. When the derivatives of the probability amplitudes of the upper states $|j\rangle$ are small as compared to the detuning from these states, the system can be described by an effective, distance-dependent, 2x2 Hamiltonian

$$H_{eff} = -\hbar \begin{pmatrix} \Omega_{aa} & \Omega_{ab} \\ \Omega_{ba} & \Omega_{bb} - \delta \end{pmatrix} \tag{4.6}$$

Where Ω_{aa} and Ω_{bb} are the Stark shifts and Ω_{ab} is the two-photon Rabi-frequency. These quantities are expressed as

$$\Omega_{aa} = \frac{1}{2}\sum_q a_q |E_q|^2, \tag{4.7a}$$

$$\Omega_{bb} = \frac{1}{2}\sum_q b_q |E_q|^2, \tag{4.7b}$$

$$\Omega_{ab} = \Omega_{ba}^* = \frac{1}{2}\sum_q d_q E_q E_{q+1}^* \tag{4.7c}$$

a_q, b_q and d_q are the dispersion and coupling constants and can be expressed as follow

$$a_q = \frac{1}{2\hbar^2}\sum_j \left(\frac{|\mu_{ja}|^2}{\omega_j - \omega_a - \omega_q} + \frac{|\mu_{ja}|^2}{\omega_j - \omega_a + \omega_q}\right) \tag{4.8a}$$

$$b_q = \frac{1}{2\hbar^2}\sum_j \left(\frac{|\mu_{jb}|^2}{\omega_j - \omega_b - \omega_q} + \frac{|\mu_{jb}|^2}{\omega_j - \omega_b + \omega_q}\right) \tag{4.8b}$$

$$d_q = \frac{1}{2\hbar^2}\sum_j \left(\frac{\mu_{aj}\mu_{jb}}{\omega_j - \omega_b - \omega_q} + \frac{\mu_{aj}\mu_{jb}}{\omega_j - \omega_b + \omega_q}\right) \tag{4.8c}$$

The two level system is governed by the equations

$$\frac{\partial \rho_{aa}}{\partial \tau} = i(\Omega_{ab}\rho_{ab}^* - \Omega_{ab}^*\rho_{ab}) + \gamma_{||}\rho_{bb}, \tag{4.9a}$$

$$\frac{\partial \rho_{bb}}{\partial \tau} = -i(\Omega_{ab}\rho_{ab}^* - \Omega_{ab}^*\rho_{ab}) - \gamma_{||}\rho_{bb}, \tag{4.9b}$$

$$\frac{\partial \rho_{ab}}{\partial \tau} = i(\Omega_{aa} - \Omega_{bb} + \delta + i\gamma_{\perp})\rho_{ab} + i\Omega_{ab}(\rho_{bb} - \rho_{aa}) \tag{4.9c}$$

The quantities ρ_{ij} are the elements of the 2x2 density matrix and $\rho_{aa} + \rho_{bb} = 1$ and the $\gamma_{||}$ and $\gamma_{\perp}$ are the population decay rate of the state $|b\rangle$ into the state $|a\rangle$ through irradiative process and the decay rate of the coherence associated with the non-allowed transition $|b\rangle \leftrightarrow |a\rangle$, respectively. Under steady state condition the equations 4.9a and 4.9b are reduced to a single equation.

Eq. 4.9a & 4.9b $\Rightarrow i(\Omega_{ab}\rho^*_{ab} - \Omega^*_{ab}\rho_{ab}) + \gamma_{||}\rho_{bb}$, from this we can write

$$\rho_{bb} = \frac{-i(\Omega_{ab}\rho^*_{ab} - \Omega^*_{ab}\rho_{ab})}{\gamma_{||}} \tag{4.10}$$

Under steady state condition from Eq. 4.9c, ρ_{ab} can be expressed as follows

$$\rho_{ab} = \frac{-\Omega_{ab}(\rho_{bb} - \rho_{aa})}{(\Omega_{aa} - \Omega_{bb} + \delta + i\gamma_{\perp})} \tag{4.11}$$

Substitute the Eq.4.11 into the Eq.4.10 and solve the equation for ρ_{bb} gives

$$\rho_{bb} = \frac{|\Omega_{ab}|^2 \frac{2\gamma_{\perp}}{\gamma_{||}}}{\delta^2_{\Omega} + \gamma^2_{\perp} + |\Omega_{ab}|^2 \frac{2\gamma_{\perp}}{\gamma_{||}}} \tag{4.12}$$

Substituting this value into the equation Eq. 4.11 and utilizing the $\rho_{aa} + \rho_{bb} = 1$, the steady state coherence absolute value can be expressed as

$$|\rho_{ab}| = \frac{|\Omega_{ab}|\sqrt{\delta^2_{\Omega} + \gamma^2_{\perp}}}{4|\Omega_{ab}|^2 \frac{\gamma_{\perp}}{\gamma_{||}} + \delta^2_{\Omega} + \gamma^2_{\perp}} \tag{4.13}$$

where $\delta_{\Omega} = \delta + \Omega_{aa} - \Omega_{bb}$. The state has the resonance nature, where the two photon detunings are very small or even zero.

The decay rates can be neglected completely under the existence of the adiabatic states which are given by $|\pm\rangle = \cos\theta^{(\pm)}|a\rangle + \sin\theta^{(\pm)}e^{-i\phi}|b\rangle$. The coherence of the superposition of levels $|a\rangle$ and $|b\rangle$ in the dressed eigen states $|\pm\rangle$ can be expressed as

$$\rho^{\pm}_{ab} = \pm\frac{\Omega_{ab}}{\sqrt{(\Omega_{aa} - \Omega_{bb} + \delta)^2 + 4|\Omega_{ab}|^2}} \tag{4.14}$$

The signs ± represents the phased and anti-phased states respectively, which can be determined by the sign of the two photon detuning δ. In the phased state the coherence ρ_{ab} and the two-photon driving Ω_{ab} are in phase with each other where as in the anti-phased state these are out of phase with other. The stark shifts of the Raman states under large one-photon detunings are equal $\Omega_{aa} \approx \Omega_{bb}$. Which will simplify the Eq. 4.14 as $\rho_{ab}^{\pm} = \pm\frac{\Omega_{ab}}{\sqrt{\delta^2+4|\Omega_{ab}|^2}}$. The coherence can reach its maximum value $\frac{1}{2}$ for $|\delta| << |\Omega_{ab}|$. This can be realized for small two photon detunings and strong driving fields.

In the adiabatic case the maximum coherence is limited to a short time intervals. Maintaining the high coherence for long time intervals is an attractive feature. On the other hand, the steady state coherence reach its maximum value at the the detunings $\delta_\Omega = \pm\sqrt{|\Omega_{ab}|^2\frac{\gamma_\perp}{\gamma_{||}} - \gamma_\perp^2}$. The maximum value of the steady state coherence is given by

$$|\rho_{max}^{steady}| = \frac{1}{4}\sqrt{\frac{\gamma_{||}}{\gamma_\perp}} \tag{4.15}$$

which means the steady state maximal coherence strongly dependent on the ratio of the effective population decay rate from the excited state $|b\rangle$ to the ground state $|a\rangle$. In the reality this value is considerably high. Lets say, the ratio is 1/4 , which will limit the maximum coherence to a value $\sim \frac{1}{8}$. Even though the steady state coherence is small compared to the adiabatic state coherence, it is sufficient for many applications in the continuous wave regime.

4.3 Experimental system

There are few ways to generate stimulated Raman components with the CW lasers, 1. High finesse optical cavity 2. Hollow core photonic crystal fibers with few micron core diameters 3. Sub micron optical fibers 4. High finesse optical micro ring resonators. All there techniques can enhance the driving lasers intensities to a values greater than $10^6 W/cm^2$. Here, we select the high finesse optical cavity to generate Raman side bands.

The experimental system to study the Raman sideband generation is shown in figure 4.2. The driving laser system to generate Raman sidebands is similar with system shown in chapter2. This system contains all the components of DFIL (Dual-frequency injection-locked) laser system and apart from these , it contains a gas cell, an Ortho to Para- H_2 conversion system, and an optical multi channel analyzer (OMA- to detect and monitor the signals). As shown in the figure the out put of the DFIL laser system is coupled to the high finesse cavity by using suitable mode matching lens. This cavity simultaneously acts as a reference cavity to the DFIL laser system, as well as the enhancement cavity to generate CW Raman. The Raman driving laser fields and the locking fields are orthogonal to each other, to avoid the locking instability. The high finesse cavity is kept in side a gas cell and the cell is filled with the para-H_2 gas medium. The gas cell and cavity are kept at the room temperatures.

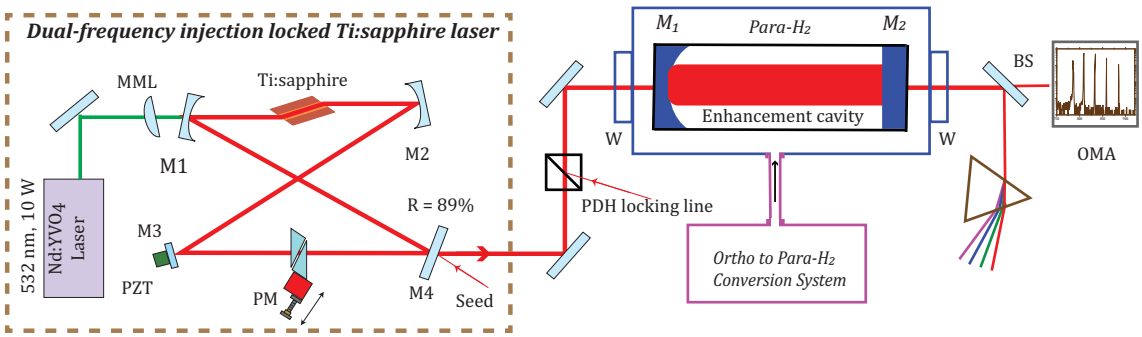

Figure 4.2: Experimental system to study the Raman sideband generation. W, window; M_1 and M_2; cavity mirrors, BS; beam splitter, OMA; optical multi-channel analyzer.

4.4 Dispersion effect on coherent Raman sidebands generation

There are few requirements to generate multiple Stokes and anti-Stokes Raman; 1. Stable confinement of the driving lasers with the high finesse cavity 2. Confinement of the generated sideband frequencies with the high finesse cavity 3.The generation process should satisfy the phase matching conditions. About 1^{st} requirement, we will

discuss in the later section. To fulfill 2^{nd} and 3^{rd} requirements, it is necessary to mange the dispersion.

The dispersion mainly comes from two components, one is the Raman active medium, which is the para- H_2 gas. The second is the highly reflective cavity mirror coatings. Because of these requirements, generation of multiple coherent Raman components with CW lasers is a challenging problem. Generation of multiple Stokes components (only) through cascading Raman process doesn't need to satisfy the phase matching condition. But, the generated components do not follow any phase relation among them. For many applications, it is necessary to have a definite phase relationship, such as arbitrary optical waveform generation etc., The anti-stokes components only can generate through FWM process and it requires to satisfy the phase matching condition. The wave vector mismatch is given by the equation, $\Delta k = 2k_0 - k_1 - k_{-1}$ where k_0, k_1, k_{-1} are the wave vectors corresponds to the pump, stokes and anti-stokes frequencies respectively. The wave vector in a dispersive media is defined as, $k(\omega) = 2\pi n(\omega)/\lambda$, where $n(\omega)$ is the frequency dependent refractive index of the Raman active medium. In the case of para-hydrogen gas, the wave vector mismatch involved in the coherent stokes (830 nm) and anti-Stokes (784 nm) generation process corresponding to a pump laser at 806 nm (rotational transition $J = 0 \leftrightarrow J = 2$) is estimated to be $\Delta k = -0.065 m_{-1}$ at 1atm gas pressure (at room temperature). The corresponding phase slip lengths are much larger than the cavity length of 6 cm. The Stokes and anti-Stokes frequencies, which are generated with a fixed modulation frequency of the molecular coherence should satisfy the cavity resonant conditions. But the existing dispersion is made this system much complex. As mentioned previously, Raman generation in the cavity is not only the dispersion of the gas medium but also the dispersion introduced by the cavity mirror coatings. The resultant FSR of the cavity in a dispersive media can be expressed by the following equation,

$$FSR_{(\omega)} = \frac{c}{2(Ln_g(\omega) + c\beta_{mirror}(\omega))} \tag{4.16}$$

where, c is the speed of the light, n_g is the group refractive index of the intra-cavity medium, L is the length of the optical cavity,β_{mirror} is the group delay given by the one reflection of the cavity mirror.

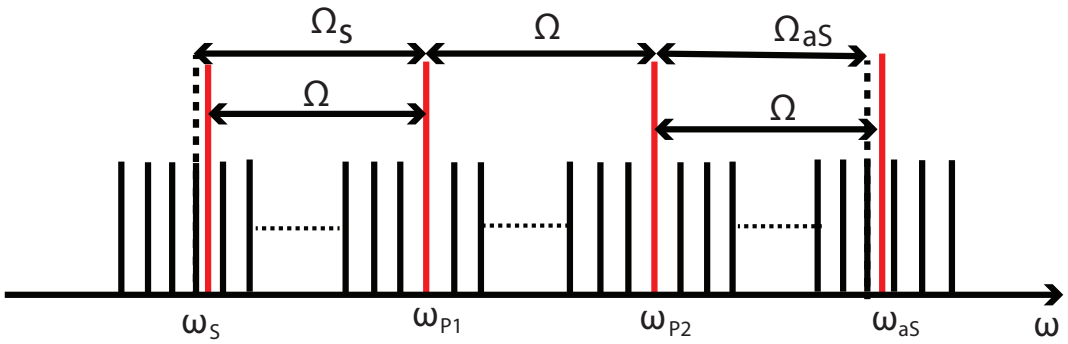

Figure 4.3: Effect of frequency dependent free spectral range (FSR) in the generation of Stokes and anti-Stokes fields inside the Raman cavity

The frequency dependent FSR is made the stokes and anti-Stokes frequency modes off resonant with the cavity. Which means the Stokes and anti-Stokes fields can not be amplified inside the cavity. In the case of two frequency pumping case it can be explained as shown in figure 4.3. The frequencies ω_{P1} and ω_{P2} are the driving laser frequencies. Let's assume these two frequencies are coupled to the optical cavity. Now fill the cavity with the Raman active medium and it will introduce the dispersion, which will effect the two photon Raman detuning (Ω). In this case, it is possible to get a desired two photon detuning by adjusting the cavity length. Now, what will happen for the generated sideband frequencies? Because of the frequency dependent FSR, for a fixed two photon detuning (Ω), the modes of the Stokes and anti-Stokes are deviated from the cavity resonances as shown in the figure. This deviation effect the amplification of Stokes and anti-Stokes fields inside the Raman cavity, as a result no Stokes and anti-Stokes are observed at the the output field. To realize the Stokes and the anti-Stokes generation in the cavity, it is necessary to compensate the effective dispersion. It is possible with the aid of the special cavity mirrors, in which the cavity mirrors introduce a negative delay that can compensate the dispersion of the gas.

4.5 Results and discussions

As mentioned in the previous section the first requirement to realize the Raman based molecular modulator using an optical cavity is the strong confinement of the two driving laser frequencies with the high finesse cavity. In the current study, the DFIL laser output is coupled to the same enhancement (reference) cavity to which the two driving laser frequencies were locked as shown in the laser system figure 2.6 and figure 4.2. The DFIL laser output frequencies are spatially overlapped with each other and have similar divergence profiles. These features are made easy to deal with the dual frequency beam, where as using the two independent laser systems to realize the perfect spatial overlap is difficult. The DFIL laser is coupled to the high finesse cavity using a suitable mode matching lens. In this way we have realized the stable dual frequency coupling with a coupling efficiency $\sim$ 80%. In this case the two photon detuning frequency can be adjusted by tuning the cavity length using the PZT attached to the one of the cavity mirror. We have realized the triple resonant condition that is the selected two frequencies are resonant with the Raman transition frequency, resonant with the high finesse cavity and also resonant with the power oscillator cavity simultaneously. Which means, the first requirement has fulfilled by the stable coupling of the two driving laser frequencies to the high finesse cavity.

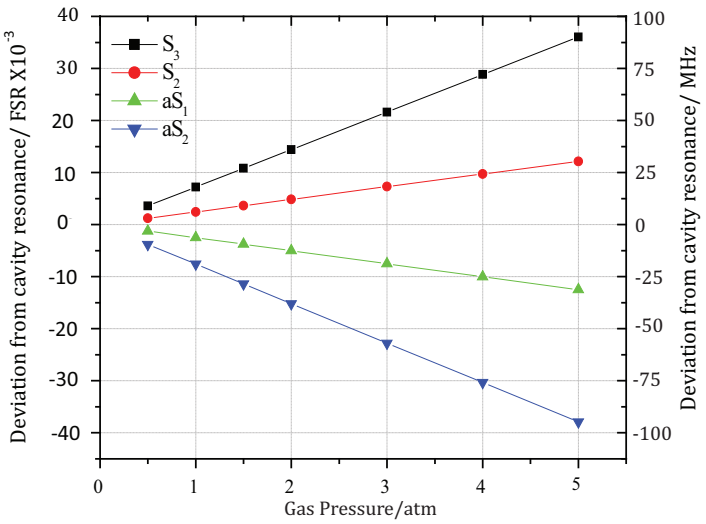

Figure 4.4: Raman medium dispersion and offresonant of Stokes and anti-Stokes

Now the next requirement is the dispersion compensation at the pump and side-band frequencies. For this purpose, at first, estimated the dispersion effect on the resonances of the generated frequencies. The results are shown in figure 4.4. In this case only the gas dispersion was considered [10], and mirrors are considered to be as the ideal mirrors without any dispersion. At 2 atm gas pressure the deviation of the second Stokes and first anti-Stokes are 6 MHz each (in this case pump and Stokes-1 are the driving lasers). This value is far from the cavity allowed line width of 170 kHz corresponds to the cavity finesse of ∼15,000. It is necessary to compensate the dispersion introduced by the gas. Not only for the purpose of the resonances but also for the compensation of the phase slips introduced by the dispersion of Raman medium. For this purpose, we select the cavity mirrors with a negative group delays, which will introduce the negative group delay that can cancel the dispersion introduced by the Raman medium. In reality, it is difficult to get the mirrors with the required precision for a fixed gas density. Because of this reason, the gas density was varied from 0.1 to 4 atm.

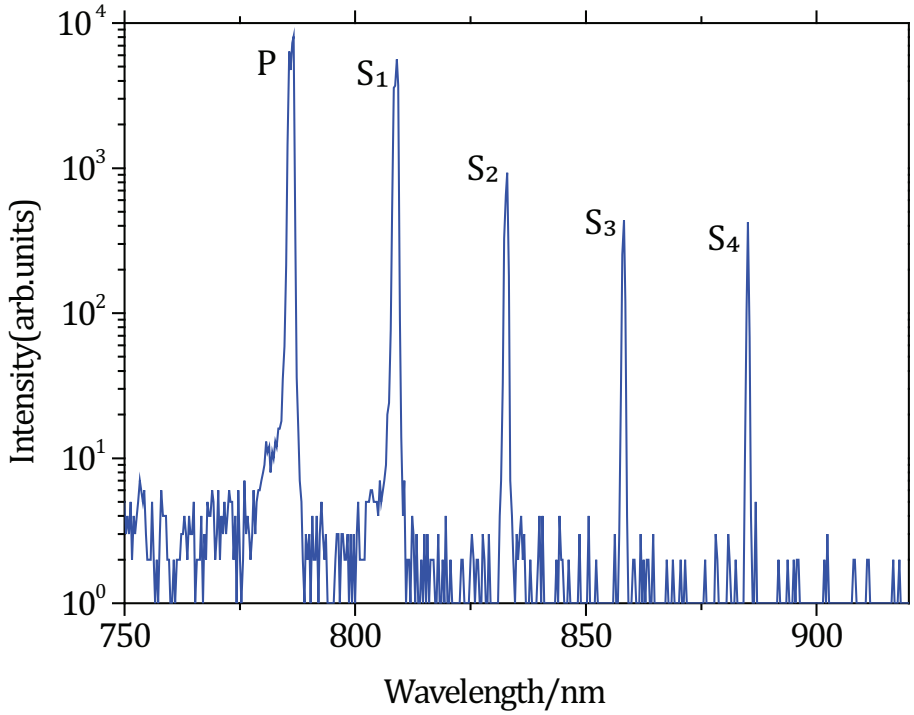

Figure 4.5: Multiple rotational Raman sideband generation by single frequency driving (784nm)

Raman generation with a single driving frequency was studied to understand dispersion effect on the phase matched anti-Stokes generation by changing the detunings and gas density. In this process, the generated Stokes frequency can be selected precisely by adjusting the cavity length with the help of PZT. It gives very fine adjustment of the two photon detuning, with a precision better than 10 MHz (relative frequency). Now the high power injection locked Ti:sapphire laser was introduced into the cavity and monitor the Raman frequency components, using the Optical-Multichannel- Analyzer. At first, the Raman generation with 784 nm laser was studied. The side band components are monitored by changing the gas pressure on the order of 0.1 atm. Multiple Stokes sidebands up to 4th order Stokes component are observed at 784 nm driving laser. The optical spectrum was shown in figure 4.5. In this case, no anti-Stokes components were observed. The number of Stokes components are limited by the mirror coatings (both the mirrors have high reflectivities

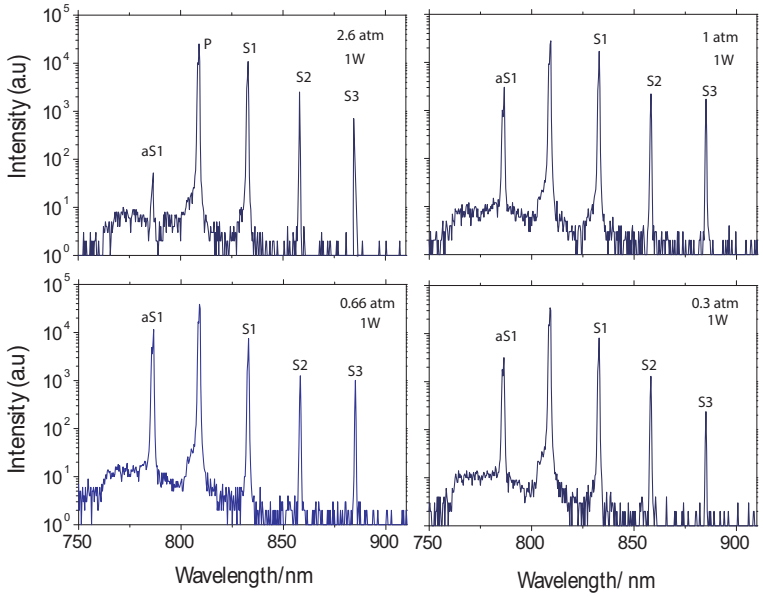

Figure 4.6: Density dependent Raman sideband generation by single frequency driving (806 nm)

from 700nm-900nm, Appendix-B).

To find the best phase matching condition, the driving laser was changed to 806 nm laser. Now the high power injection locked 806 nm was coupled to the Raman cavity and monitor the Raman sideband generation. The experiment started from 4 atm para-H2 gas pressure (room temperature), at 4 atm multiple Stokes components were observed but no considerable anti-Stokes signal was observed. Later the gas pressure was changed in steps of 0.1 atm and monitored the Raman components. Around 3 atm considerable anti-Stokes signal was observed and it has improved further by reducing the gas density. Strong anti-Stokes signal was observed at 1 atm gas pressure. Few of the results are shown in figure 4.6. This signal is an indication of the dispersion compensation of the gas medium with the negative mirror coatings. In this case the number of anti-Stokes components are limited by the dispersion compensation region.

In the case of 806 nm driving laser, there has observed strong anti-Stokes emission at 784nm along with the multiple Stokes components. But in the case of 784

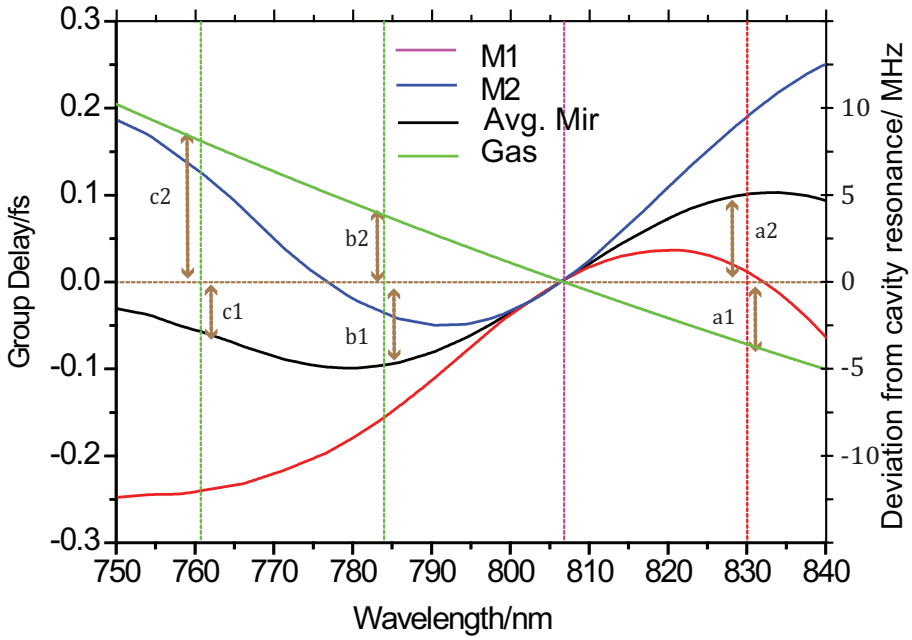

Figure 4.7: Dispersion introduced by the para-H2 gas and cavity mirrors.

nm driving laser no anti-stokes signal was observed. The reason for this was the resultant dispersion at the Stokes and anti-Stokes frequencies. The estimated dispersion of the mirrors (Data from the manufacturer is shown in appendix-C) and the gas medium [10] at Stokes and anti-Stokes frequencies are shown in figure 4.7. In the case of the pumping laser 806 nm, the dispersion introduced by the mirror coatings were matched with the dispersion introduced by the gas medium at the Stokes (830 nm) and anti-Stokes frequencies (784 nm), where as in the case of the 784 nm driving laser, there is a considerable dispersion existed at the Stokes and anti-Stokes frequencies. In reality, perfect compensation of the dispersion over a broad frequency region is difficult. Predictable dispersion values with sub-femtosecond precision are still difficult to achieve.

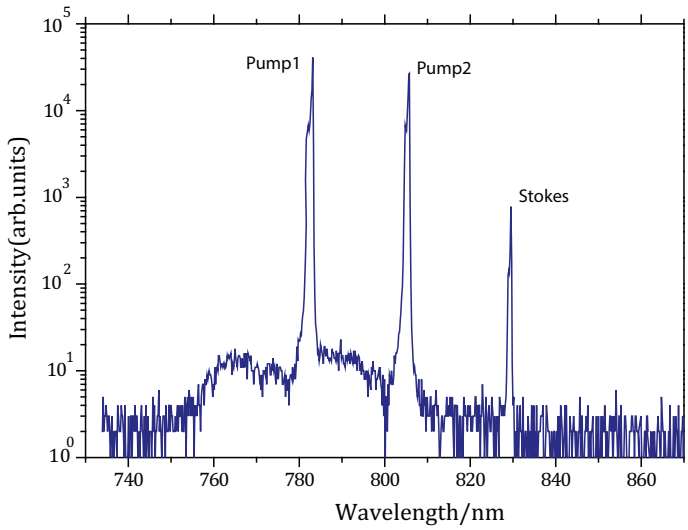

Figure 4.8: Dual-frequency pumped Raman generation

Now we fix the parameters, where the efficient anti-Stokes sideband was generated. At this state, dual-frequency injection-locked laser was introduced. The results are shown in figure 4.8. Pump1 (784 nm) and pump2 (806 nm) are the driving lasers and the signal at 830 nm was the coherently generated Stokes component. In this case, there wasn't observed any anti-Stokes frequencies. The reason was similar to the single frequency driving 784nm case. Where the group delays introduced by the gas medium at the pump1, pump2 and first Stokes frequencies were compensated by the cavity mirrors coatings, which was shown in figure 4.7. Later we checked the nature of the generated Stokes frequency. For this, we cut the one of the driving frequency (pump1) and observed that no Stokes frequency was generated. Which means the Stokes frequency was generated through four wave mixing process (FWM), by utilizing the coherence created by the two driving laser frequencies.

From this study we understand, it is necessary to compensate the dispersion to a wide optical region precisely (with subfemto-second effective group delays), to generate wide coherence spectrum.

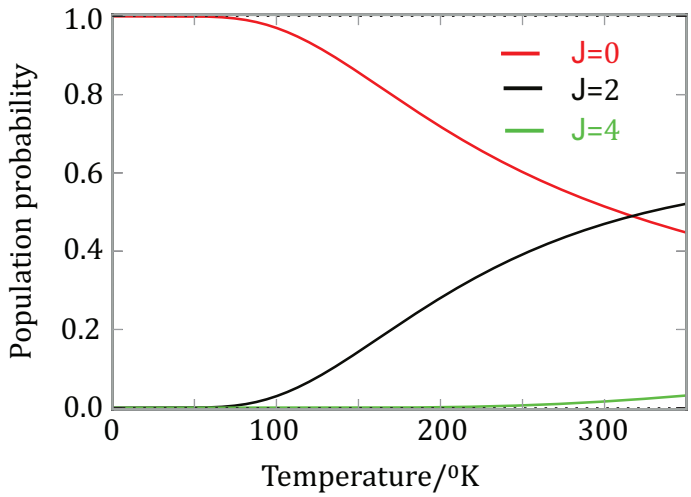

Figure 4.9: Temperature dependent population density of Para-H_2 rotational energy levels

All the above experiments were dealt with the J=0 to J=2 rotational transition. But, at room temperature, the molecules are not only in the ground state also have considerable probability distribution in the first excited state also. As shown in the figure 4.9, at room temperature, the fist excited state have equally probability as the ground state. To investigate the other possible transitions, we swept the Raman cavity around the two photon resonance. The cavity sweeping frequency is set to 100 Hz and the sweeping range is 25 MHz around the pump resonance position. we observed the Stokes components corresponding to the J=0 to J=2 and J=2 to J=4, and the results were shown in figure 4.10. The Stokes frequencies S1(0), S2(0), S3(0), S4(0) are the corresponding to J=0 to J=2 transition. The signal marked by P' was the Stokes corresponding to the transition J=2 to J=4 in the para hydrogen, which was the consequence of the considerable steady state population in the first excited state. Later this secondary Stokes acts as the pump and generated higher order Stokes frequencies corresponding to the transition J=0 to J=2 matched with S1' and S2'. These unwanted components can be suppressed by cooling down the Para-H2 gas to the liquid-N_2 temperature. It can greatly enhances the effective generation process.

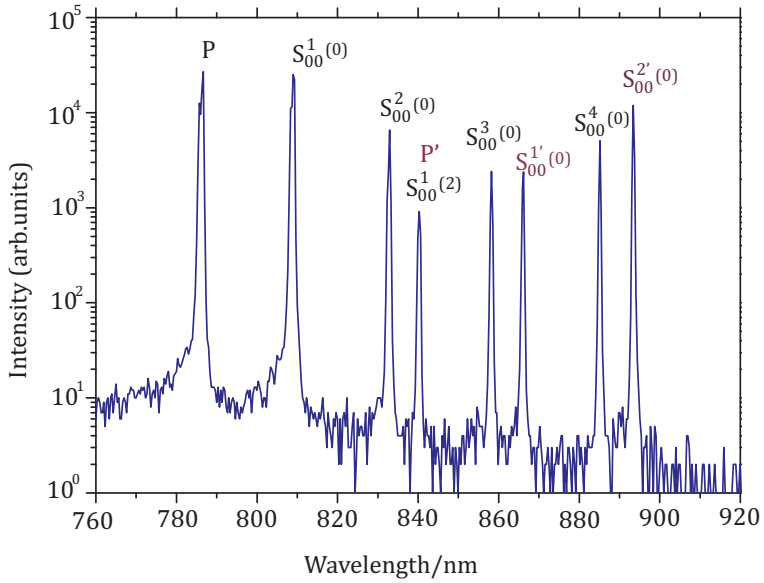

Figure 4.10: Raman generation in Para hydrogen using multiple rotational transitions

4.6 Conclusions

In this chapter, we have shown the potential application of the dual frequency laser, which played an important role in the realization of the molecular modulation phenomena. We have discussed the requirements to realize the continuous wave based coherent Raman sideband generation in the para-H_2 gas medium using high finesse optical cavity, such as stable confinement of the two driving laser frequencies and the dispersion management at the generated sideband frequencies. The stable confinement of the two driving laser frequencies was realized with the aid of the dual-frequency injection-locked laser. The dispersion was compensated by utilizing the negative group delay mirrors and by controlling the gas densities. We observed strong anti-Stokes generation through four wave mixing process. We have understand the required precision of the group delay (< 0.1 fs) to realize the broad band Raman comb, which is essential to further study the broad band Raman generation with CW lasers.

Bibliography

[1] A. Nazarkin, G. Korn, M. Wittman, and T. Elsaesser, "Generation of Multiple Phase-Locked Stokes and Anti-Stokes Components in an Impulsively Excited Raman Medium", Phys. Rev. Lett. **83**, 2560 (1999)

[2] S. Uetake, M. Katsuragawa, M. Suzuki, and K. Hakuta, " Stimulated Raman scattering in a liquid-hydrogen droplet", Phys. Rev. A. **61**, 011803 (R)(1999)

[3] J.Q. Liang, M. Katsuragawa, F. Le Kien, and K. Hakuta, "Sideband Generation Using Strongly Driven Raman Coherence in Solid Hydrogen", Phys. Rev. Lett. **85**, 2474 (2000)

[4] A. V. Sokolov, "Subfemtosecond pulse generation by molecular modulation", Ph. D thesis (2001)

[5] Deniz D. Yavuz, "A Raman approach for generating ultrashort pulses", Ph. D thesis (2003)

[6] A. V. Sokolov, D. R. Walker, D. D. Yavuz, G. Y. Yin, and S. E. Harris, "Raman generation by phased and antiphased molecular states", Phys. Rev. Lett. **85**, 562(2000)

[7] L. Meng, P. A. Roos, K. S. Repasky, and J. L. Carlsten, "High-conversion-efficiency, diode-pumped continuous-wave Raman laser", Opt. Lett. **26**, 426 (2001).

[8] S. Zaitsu, H. Izaki, and T. Imasaka, "Phase-matched Raman-resonant four-wave-mixing in a dispersion-compensated high-finesse optical cavity", Phys. Rev. Lett. **100**,073901 (2008)

[9] F. Benabid, J. C Knight, G. Antonopoulos, and P. S. J. Russell, "Stimulated Raman scattering in hydrogen-filled hollow-core photonic crystal fiber", Science **298** 399-402 (2002)

[10] E. R. Peck and Shiezen Huang, "Refractivity and dispersion of hydrogen in the visible and near infrared", J. Opt. Soc. Am., **67**, 1550 (1977)

CHAPTER 5

Ultrafast optical pulse train at 125 THz repetition rate based on the optical frequency division technology

5.1 Introduction

In the preceding chapter, a potential application of dual-frequency injection-locked (DFIL) laser in the development of molecular modulator was described. The DFIL laser system can be used as the multiple frequency laser source as well as the single frequency laser source with similar basic laser features. In this chapter an application of the single frequency injection-locked laser in the optical frequency division is shown. Frequency division in the optical region has great interest because of its advantage of coherently linking independent laser oscillators [1–4]. These frequencies can be used as a broadband coherent laser light source in the frequency domain and also, can be used as an ultra-fast pulse train in the time domain by controlling the phases and amplitudes. By using this technique the pulse repetition rates as high as 100 THz can be realized.

5.2 Concept of optical frequency division

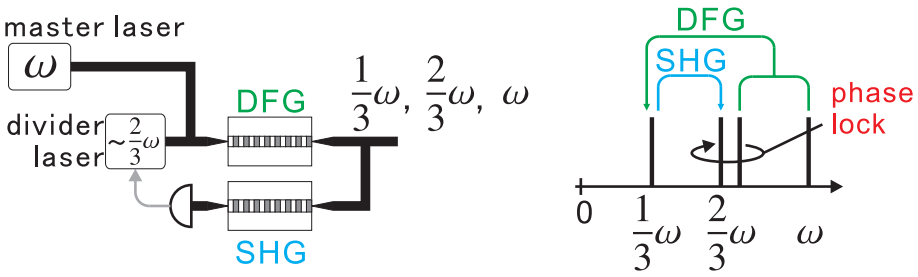

Figure 5.1: Conceptual schematic of optical frequency division technique

The importance of optical frequency division is to generate phase locked harmonic frequencies in a broad frequency region including the fundamental frequency. For this purpose, two laser frequencies are selected as the master laser (ω) and the divider laser ($\frac{2}{3}\ \omega$) as shown in figure 5.1. These frequencies are employed to a difference frequency generation (DFG) to generate fundamental frequency ($\frac{1}{3}\ \omega$). Then the fundamental frequency ($\frac{1}{3}\ \omega$) employed to second harmonic process (SHG) to generate $\frac{2}{3}\ \omega^1$. Now, beat note is created between the $\frac{2}{3}\ \omega$ and $\frac{2}{3}\ \omega^1$ and this signal is used as the error signal to feedback to the divider laser ($\frac{2}{3}\ \omega$) to obtain the three phase locked frequencies with exact frequency ratios 1:2:3. Also, It is possible to generate the other higher harmonic frequencies, such as 4^{th}, 5^{th}, and so on. These phase-locked frequencies can be used as the broad band coherent laser source in the frequency domain and ultra-fast optical pulse train in time domain.

In the optical frequency division based phase locked high harmonics generation process, the master laser power must be high enough, because this frequency later converted into the other harmonic frequencies.

5.3 Overview of amplitude and phase manipulations

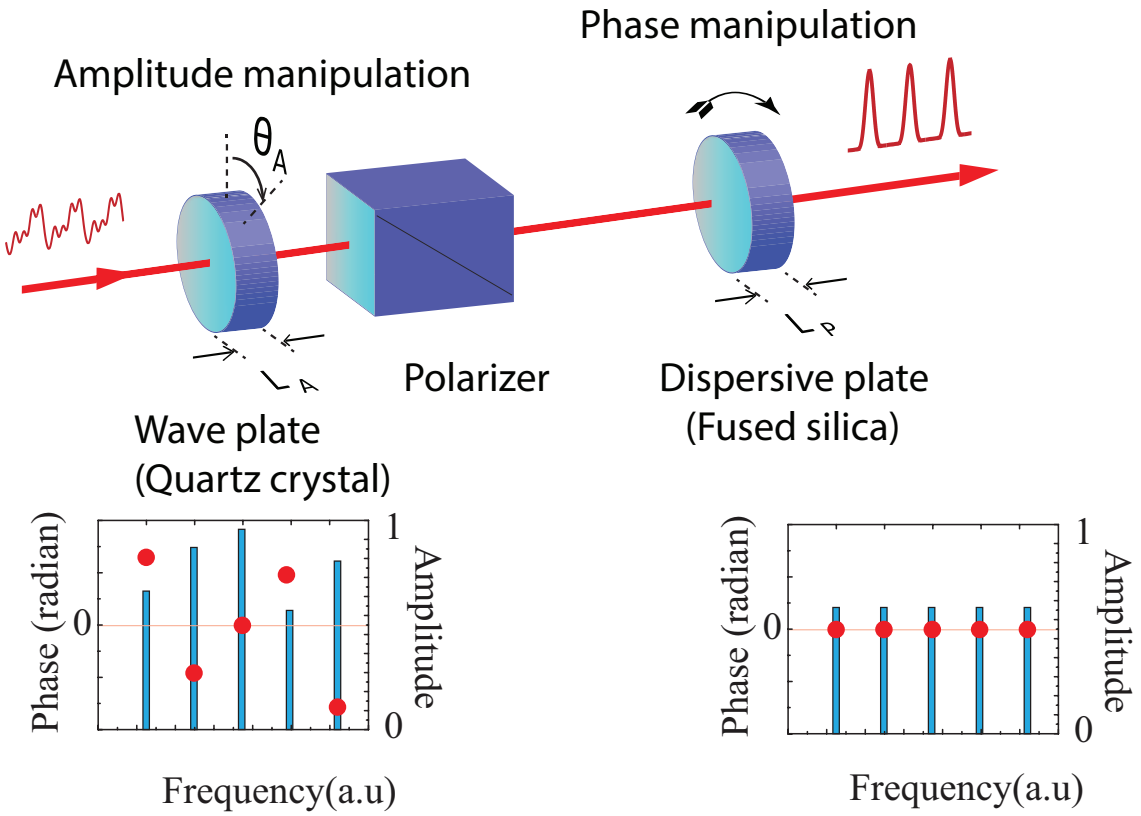

Figure 5.2: Schematic of arbitrary manipulation of amplitude and phases of a discrete frequencies

There are few ways to control the amplitudes and phases of a broad band discrete frequency spectra [5] with the use of liquid crystal spatial modulators [6], line by line controlling of spatially separated frequencies [7, 8] and by using the combination of a uni-axial birefringent material and a polarizer [9]. Freely controllable phases and amplitudes of a broad band spectrum of discrete frequencies is one of the technique to obtain a arbitrary optical wave form in time domain. Figure 5.2 shows the schematic of the arbitrary manipulation of amplitude and phase of a discrete spectra. The system consists of two parts; one is amplitude manipulation part, it consists of a uni-

axial birefringent material (acts as a wave plate) and a polarizer. The combination of these two components act as an amplitude manipulation system. The working principle can be explained by the given formula;

$$|I_m| = |E^y{}_m|^2 = 1 - \sin^2 2\theta_A \sin^2 (\Gamma_m/2) \tag{5.1}$$

where $\Gamma_m = [n_s(\omega_m) - n_f(\omega_m)]\omega_m \frac{L_A}{c}$. n_s, n_f, ω_m, c, andL_A are the refractive index at slow axis, at fast axis, angular frequency, speed of light in vacuum and length of the crystal respectively.The second part is phase manipulation system which consists of a dispersive material (Fused silica). By changing the thickness of this material the relative phases can be controlled, because of the different frequencies feel different optical path lengths inside the dispersive material. The combination of amplitude and phase control systems applying simultaneously on a broad band discrete spectra will lead to controllable optical waveform in time domain which is called arbitrary optical wave form.

5.4 Experimental system

As shown in figure 5.3, the experimental system consists of three parts 1) 2f and 3f laser systems 2) Array of PPLN waveguides including phase locking system 3) Optical pulse shaping system. The 2f laser is a 1201nm ECDL followed by a tapered amplifier (Toptica). It can deliver maximum of 1W output power. The 3f laser is 801nm injection locked Ti:sapphire laser , which is same as the DFIL laser experimental system shown in the chapter2, except the laser is operated at single frequency injection locking. It can deliver maximum of 3W output power at 801nm.The output of the injection locked Ti:sapphire laser coupled to a single mode fiber and then introduced into the PPLN1 wave guide together with the 1201nm (2f) laser to generate 2403nm (1f) through difference frequency generation. Now, part of the 1f, 2f frequencies were spatially separated and 2f beam was introduced to a frequency shift of -95 MHz with

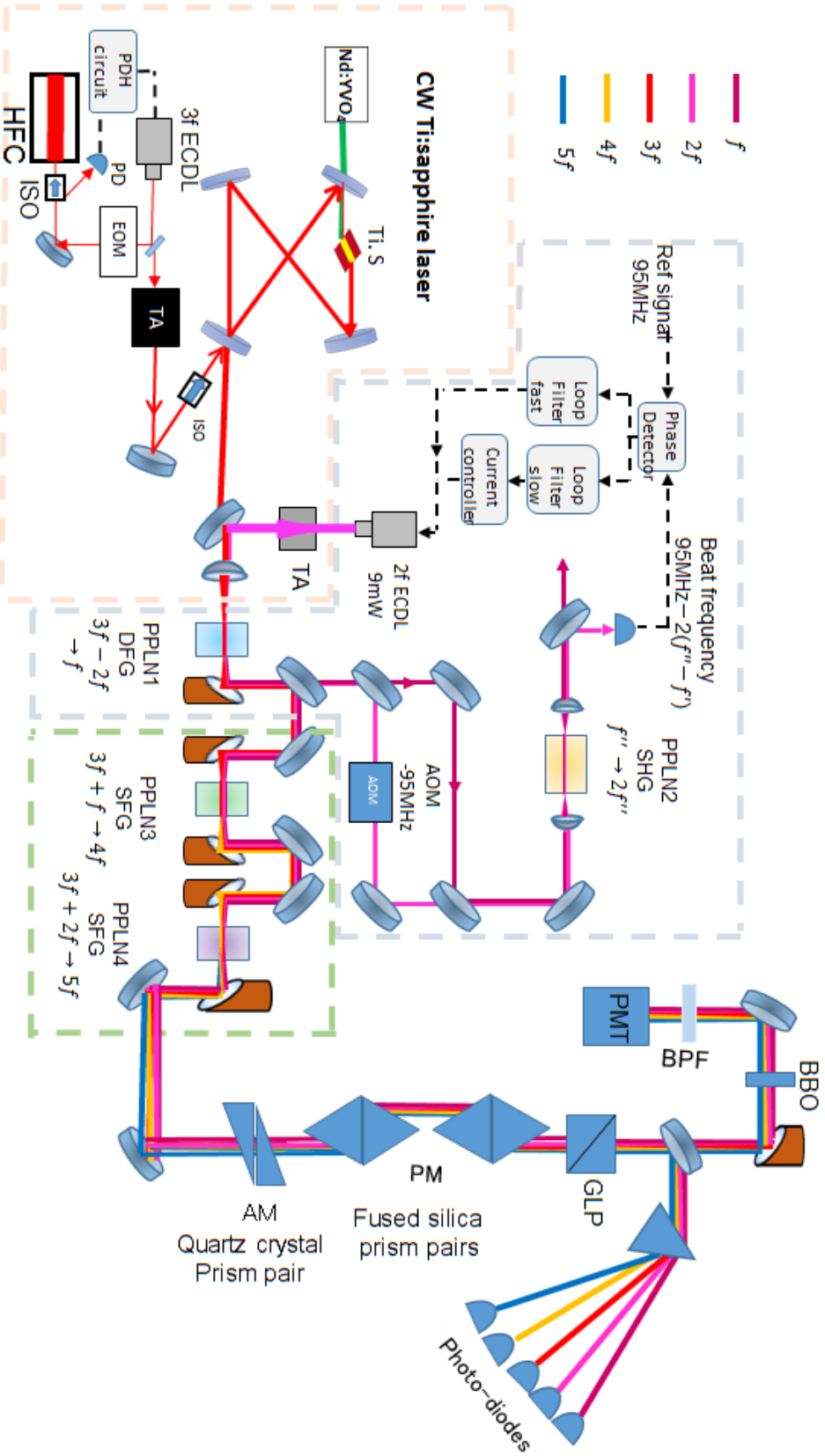

Figure 5.3: Illustration of phased locked harmonics generation system and optical pulse train generation experimental system

the help of a acoustic optical modulator (AOM) and recombined with the 1f and introduced into the PPLN2. The PPLN2 was designed to generate second harmonic (SHG) of 1f frequency (2f"). The beat signal between the 2f" and frequency shifted 2f (2f') was detected by a photo detector and was used for the feedback to the 2f laser diode through phase lock loop to obtain the phase locked three frequencies. More detailed experimental system of phase locked harmonics generation is illustrated in the ref. [10, 11]

The phase locked frequencies f1, f2, f3 are introduced into the PPLN3, PPLN4 wave guides to generate 4f (1f+3f) and 5f (2f+3f) frequency beams through the sum frequency generation. Now the five phase locked harmonics are co-axially generated after the PPLN4 wave guide as shown in the experimental system.
Now the co-axial beam of five harmonics are passing through a quartz prism pair which acts as wave-plate. The combination of this wave-plate and the Glan-laser polarizer acts as the amplitude manipulator. The fused silica prism pairs acts as the phase manipulator.These amplitude and the phase manipulations of the phase locked harmonic frequencies leads to the arbitrary optical wave form in the time domain. Amplitudes of the harmonic frequencies are measured with the independent photo detectors after dispersing into the individual frequencies with the help of dispersive prism. To determine the phases of the harmonics, these frequencies are focused on a beta barium borate (BBO) crystal and monitored the interference between possible SFGs and SHGs with the help of photo multiplier tube.

5.5 Results and discussion

We started the experiment with a 1.6 W power of master laser (3f) and a 200 mW power of divider laser (2f). The two frequencies are combined by using a dichroic mirror and coupled to the PPLN1. After all the above mentioned optical processes, we have obtained five phase locked frequency components spanning from 2403 nm to

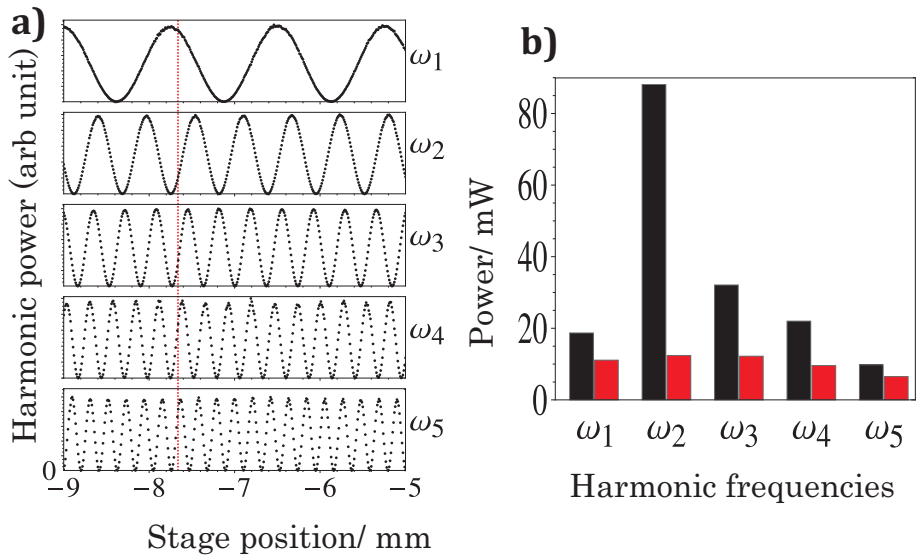

Figure 5.4: Harmonic powers before and after amplitude manipulation

480 nm. The total bandwidth of the optical spectrum is 500 THz. Each harmonic frequency has high spectral purity and maintained constant phase relation. Now this this broad optical frequency spectrum employed to amplitude and phase manipulation to obtain ultra-fast pulse train. The results are as followed below.

The results obtained in the amplitude manipulation is shown in figure 5.4b. The Black bars represent the power distribution before the AM quartz prism pair and the power of the frequencies components were distributed randomly. But, it is necessary a desired power distribution to obtain an arbitrary optical waveform or a short pulse. To manipulate the amplitudes of the each frequency, we utilized the combination of quartz crystal prism pair and the Glan-laser polarizer. By changing the insertion length of the prism which was mounted on the motorized translation stage and monitored the powers of the each harmonic individually by separating the frequencies using a dispersive prism. The results are shown in figure 5.4 a, each harmonic frequency power was sinusoidally varies as a function of the prism thickness. From this it was understood that arbitrary power combinations of the harmonic frequencies were realized for the few mm thickness change. The dotted vertical line represent the position

of the target power distribution. The power distribution at the point is represent by red bars in figure 5.4b. In this case, our desired flat profile was realized.
Now come to the phase manipulation of the harmonic frequencies. This was done by simply controlling the optical pass lengths in the dispersive media. To get the relative phase information of the harmonic frequencies, all the frequencies were focused on a BBO crystal of thickness $10\mu m$ to obtain 6f and 7f frequencies through SFG and SHG processes. The interference signals of the 6f frequencies and 7f frequencies were selected by inserting a band pass filter and detected the signal with a photo-multiplier-tube. The interference signal amplitudes as a function of the prism insertion lengths were recorded with an oscilloscope and shown shown in figure 5.5a. The dotted black vertical line represents the optimum position, where both the inference signals were at their maxima. The corresponding phases of the harmonic frequencies are shown in the figure 5.5b, where the red circles represent the phases after the phase manipulation and the black triangles represent the phases before the manipulation. After the amplitude manipulation all the phases have a flat profile and the deviations are with in the phase fluctuations of the phase locking system. In this case our obtained phase distribution was close to the ideal phase distribution of the flat phases, to obtain a Fourier transform limited (FTL) short pulse in time domain.

Now from the obtained inform of the phases and amplitudes, we combined the harmonic frequencies and estimated the pulse profile in time domain. The results are shown in the figure 5.6. The dotted curves represents the shape of the wave form before optimizing the amplitude and phases of the harmonics. The blue curves represents the theoretical Fourier transform limited pulses in the ideal case and the red curves represents the estimated wave form from the experimentally measured phase and amplitude information. The estimated wave form is close to the ideal case with a pulse duration of 1.6 fs and a repetition rate of 125 THz. This is the first optical wave form generation based on the phase-locked continuous wave laser harmonic frequencies.

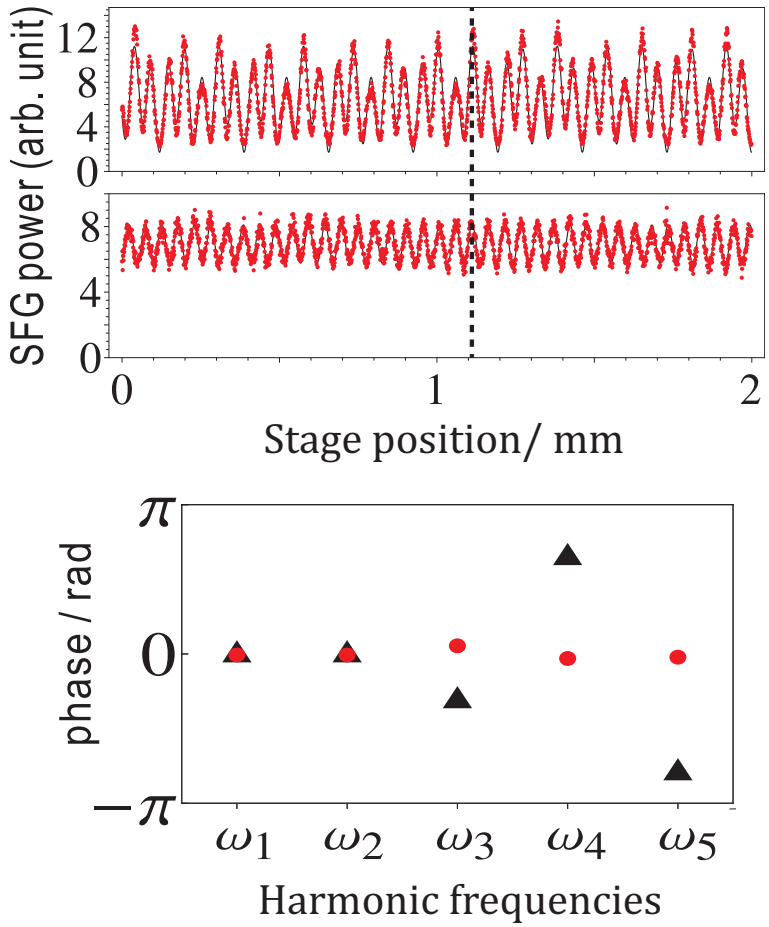

Figure 5.5: Relative phases of harmonics before and after phase manipulation

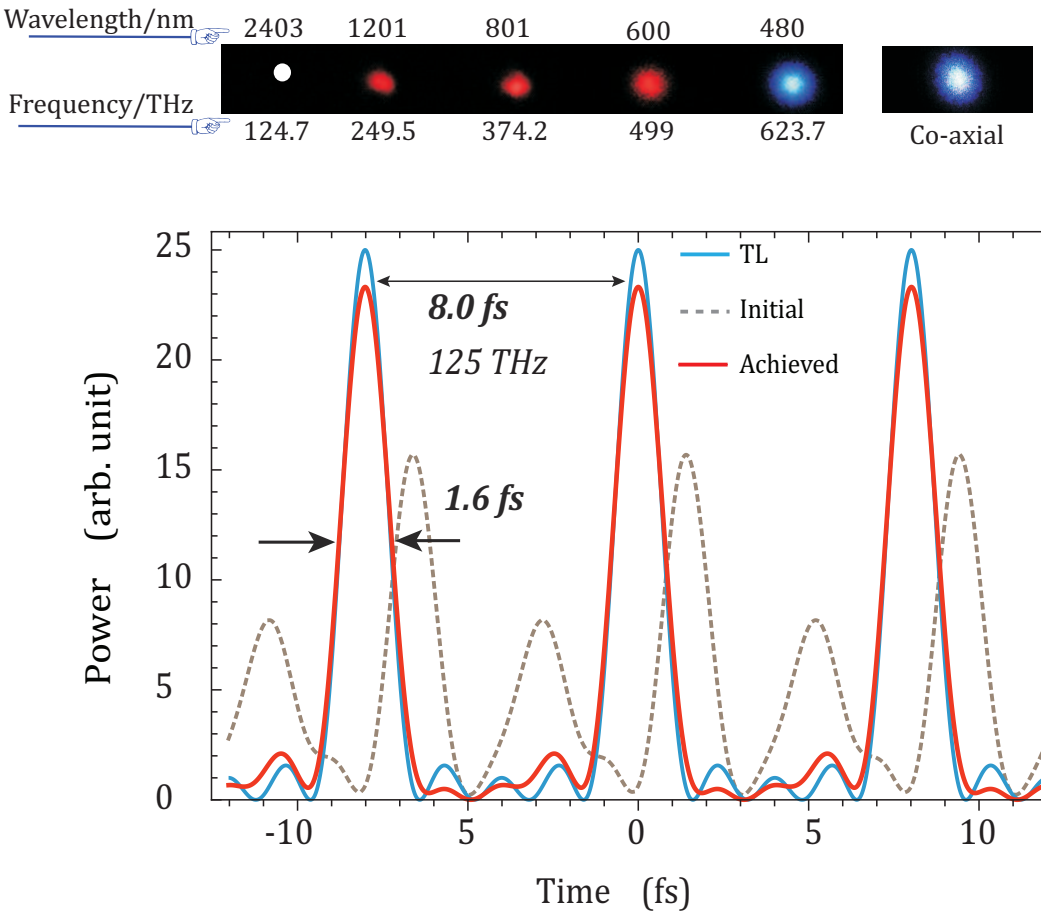

Figure 5.6: Reconstructed waveform by using the measured phases and amplitudes

5.6 Conclusions

In this chapter, we have shown the importance of high power master laser in the phase locked high harmonics generation and in the synthesis of the arbitrary optical waveform. We have described the generation of a broad band comb by employing the injection locked Ti:sapphire laser operating at 801nm as the master laser. Five phase locked harmonics spanning from 480 nm to 2400 nm were reported. We showed the arbitrary controllable amplitudes and relative phases of the broad band frequency spectrum. Later we showed that these phase locked harmonics are formed a ultra-fast optical pulse train with a repetition of 125 THz.

Bibliography

[1] H.R. telle, D. Meschede and T. W. Hansch, "Realization of a new concept for visible frequency division: phase locking of harmonics and sum frequencies", Opt. Lett. **15** , 532 (1990).

[2] T. W. Hansch, "A proposed sub-femtosecond pulse synthesizer using separate phase-locked laser oscillators", Opt. commu. **80**, 71 (1990).

[3] D. Lee and N. wong, "Tunable optical frequency division using a phase-locked optical parametric oscillator", Opt. lett. **17**, 13 (1992).

[4] R. Wynands, T. Mukai, and T. W. Hansch, "Coherent bisection of optical frequency intervals as large as 530 THz", Opt. Lett. **17**, 1749 (1992).

[5] A. M. Weiner, "Femtosecond pulse shaping using spatial light modulators", Rev. Sci. Instrum.**71**, 1929 (2000)

[6] H.-S. Chan, Z.-M. Hsieh, W.-H. Liang, A. H. Kung, C.-K. Lee, C.-J. Lai, R.-P. Pan, and L.-H.Peng, "Synthesis and measurement of ultrafast waveforms from five discrete optical harmonics", Science **331**, 1165 (2011).

[7] K. R. Pandiri, T. Suzuki, A. Suda, K. Midorikawa, and M. Katsuragawa, "Line-by-line control of 10-THz frequency spacing Raman sidebands", Opt. Express **18**,732 (2010).

[8] K. R. Pandiri and M. Katsuragawa, "A 10 THz ultrafast function generator-generation of rectangular and triangular pulse trains", New J. Phys.**13**, 023030 (2011).

[9] M. Katsuragawa and Kazumichi Yoshii, "Arbitrary manipulation of amplitude and phase of a set of highly discreate coherent spectra", PRA **95**,033846 (2017).

[10] N.S. Suhaimi, C. Ohae, T. Gavara, K. Nakagawa, F. L. Hong and M. Katsuragawa,"Generation of five phase klocked harmonics by implimenting a divide-by-three optical frequency divider", Opt. lett. **40**,5802 (2015).

[11] N.S. Suhaimi,"Generation of phase-locked high harmonics by implimenting an optical frequency divider", Ph.D thesis, (2016)

CHAPTER 6

Summary and future prospects

6.1 Summary

In this dissertation, we have discussed about the developed a new laser source and its applications in the nonlinear optical science such as molecular modulation at 10.6 THz and in the Optical wave form synthesis.The detailed summary of this dissertation is as follows.

we have demonstrated the simultaneous two frequency oscillation from a single laser cavity. we have characterized the laser basic features such as single frequency nature by using the scanning Fabry-Perot cavity and the single transverse mode profile by measuring the M^2 factor. We have reported the laser practical power stability in short time scale and relatively long time scales. DFIL laser free run power suppression as a function of injection seed power was discussed and compared with the single frequency injection locking case. As an advanced features, desirable frequency separation of the two frequencies from 10THz to 1THz have realized with this injection locking technique. Also, we have demonstrated the controllability of the relative

output power ratios of the injected frequencies as a function of the injection seed powers.

As the part of the injection locked high power laser applications in the nonlinear optical phenomena, we have studied the below mentioned optical processes.

We have studied the continuous wave based coherent Raman sideband generation in the para-H_2 gas medium by utilizing the optical cavity enhancement technique. Multiple stokes and anti-Stokes Raman generation by driving the rotational Raman transition of the J=0 $--$ > J=2 level in the case of single frequency laser pumping was reported. Enhancement of the coherent stokes emission in the case of Raman resonant two frequency laser driving and compared with the single frequency pumping case was reported. We have discussed the difficulties in the generation of broad band coherent stokes and anti-stokes generation through cavity enhancement technique. We also report the effect of the Raman medium dispersion in the broad band coherent Raman generation process.

We have discussed the importance of high power master laser in the phase locked high harmonics generation and in the synthesis of the arbitrary optical waveform. Single frequency injection locked Ti:sapphire laser operating at 801 nm was used as the master laser in the division by three optical phase locked frequencies, and later these frequency utilized to generate higher order harmonic frequencies using the array of PPLN wave guides. In this way, five phase locked harmonics were generated in the frequency span of 500THz. Freely controllable amplitudes and relative phases of the harmonics have shown. Later we showed that these phase locked harmonics are formed transform limited optical pulses in time domain. From the measured amplitudes and phases of the harmonics the reconstructed wave form has a FWHM of 1.6 fs with a pulse reputation rate of 125 THz was realized.

6.2 Future prospects

In the case of injection locked Ti:sapphire laser the current total output power is 3W. Extending this powers to multiple digit power levels will be an attractive for many optical science experiments and industry. We wants to extend this technique to a Hz level frequency stabilities [1]. It is possible to increase this output powers to double digit Watt level powers by introducing the high power pump lasers. For example, the seed frequencies after tapered amplifier are easily obtainable up to 1W. In the current case the seed to slave ratio is 1/140, which means 1W seed power easily drive the 10 W free run power. By locking the laser frequencies to a high finesse cavities with stable body with a robust feed back loops are made possible Hz level frequency stabilities.

The extend of the coherent Raman generation in the hollow core fibers can considerably reduce the required peak powers to Watt level. Driving the Raman medium by confining in the dispersion compensated few micron core hollow core photonic crystal fibers can be a efficient Raman generators [2].

The synthesized few cycle femto-second pulse technique can applied to study the optical phenomenon by confining the pulses to an optical enhancement cavity, even though the initial peak powers of the pulses are considerably low.

Bibliography

[1] D. G. Matei, T. Legero, S. Hafner, C. Grebing, R. Weyrich and W. Zhang, "1.5 μm lasers with sub 10 mHz linewidth", Phy. Rev. Lett. **118** (2017).

[2] F. Couny, F. Benabid, and P. S. Light, "Subwatt threshold cw Raman fiber-gas laser based on H 2-filled hollow-core photonic crystal fiber", Phy. Rev. Lett. **99**, 143903 (2007)

APPENDIX A

Simultaneous two frequency resonance of power oscillator cavity

To obtain stable dual frequency laser oscillation, it is necessary to stabilize the power oscillator cavity to the two frequency resonances simultaneously. There are few ways to realize the simultaneous two frequency resonance; here we select the tuning of t the optical cavity length by inserting a pair of wedges in the optical path. Even though the cavity has discrete resonances, it is possible to select frequency continuously. Figure A.1 shows the calculated longitudinal mode overlaps of the two frequencies as a function of the inserted wedge thickness. Sub figures a), b) and c) represent the longitudinal modes miss-overlap of the selected frequency pairs (783.8849 nm, 806.2823 nm), (800.0590 nm, 806.2885 nm), (801.1395 nm, 803.0041 nm) respectively. In the case of frequencies 783.8849 nm, 806.2823 nm the minimum required wedge insertion length is 50μm, where as in the case of frequencies 801.1395 nm, 803.0041 nm is 0.7mm. The period of the closest resonance positions are depended on the separation of the selected frequencies, as the separation between the frequencies decreases the number of mode overlaps in a unit length decreases. It will limit the selection of the arbitrary frequency combinations at sub nano-metre separations, where the required wedge insertion thickness are more than a centimeter.

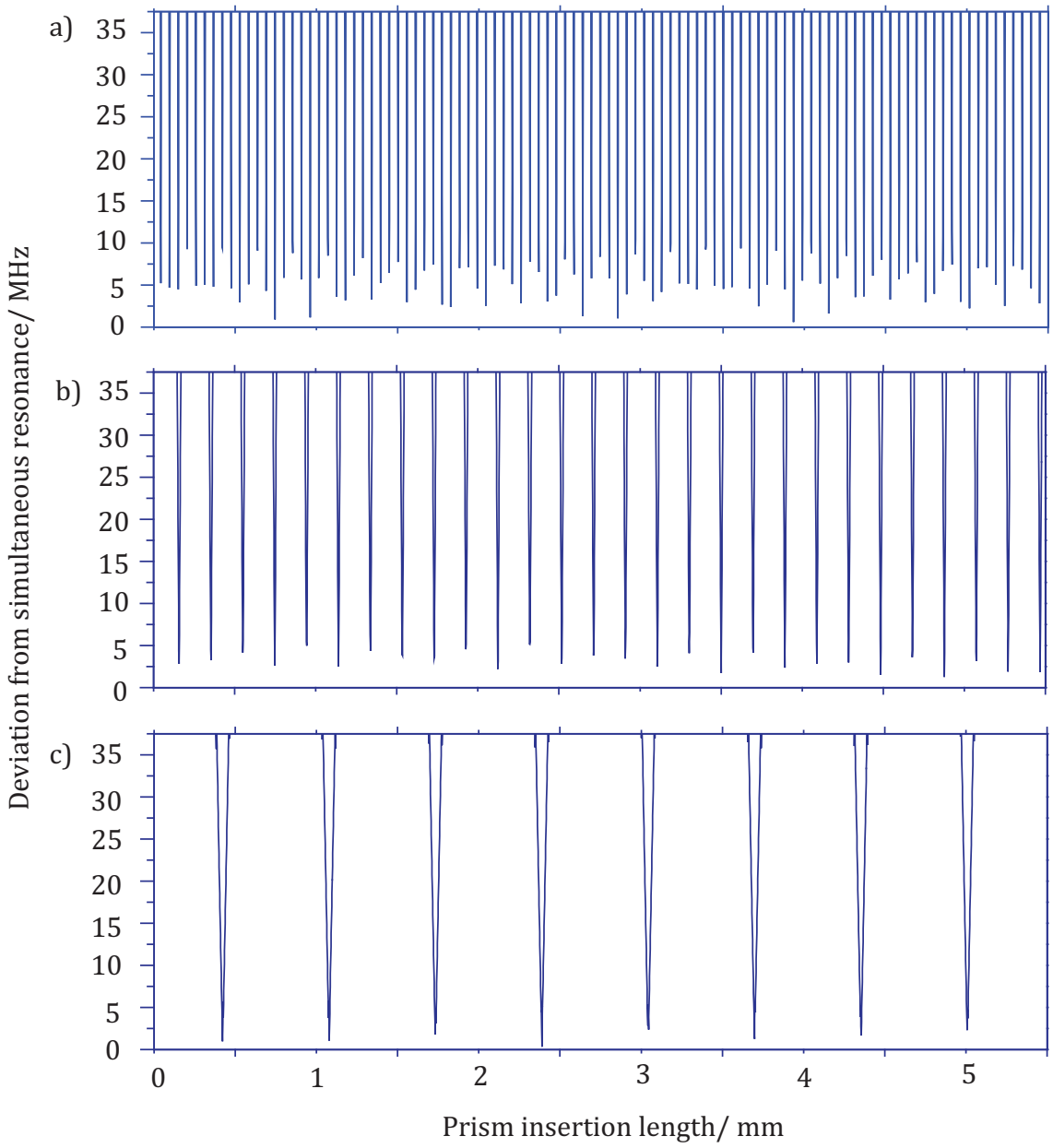

Figure A.1: Deviation from simultaneous two frequency resonance of the power oscillator cavity as function of the prism insertion length. a) , b) and c) are the resonance measurements corresponding to the frequency pairs (783.8849 nm, 806.2823 nm), (800.0590 nm, 806.2885 nm), (801.1395, 803.0041) respectively

APPENDIX B

Cavity mirrors reflectivity:

To obtain high intra-cavity powers, it is necessary to have a highly reflective low and loss cavity mirrors. Figure B. 1 represents the cavity mirror specifications that were used to study the Raman based molecular modulator. The cavity mirrors were manufactured by the Layertec company. Both the mirrors are highly reflective and the reflectivities are greater than 99.9 % over a range 700-900 nm. The corresponding cavity finesse was ∼15,000 at the both pump wavelengths (784 nm and 806 nm).

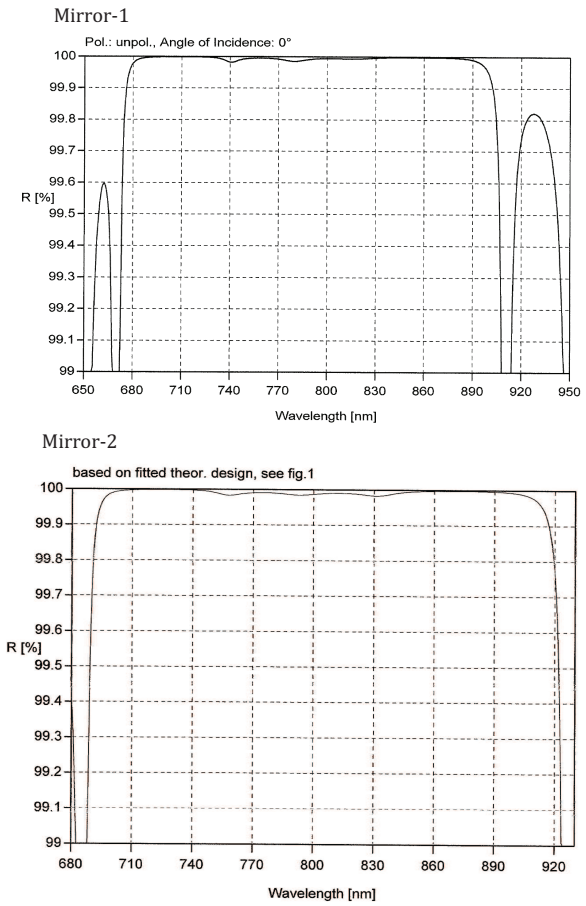

Figure B.1: Raman cavity mirror refelectivities; specifications given by Layertec Ltd

APPENDIX C

Mirror coatings

To generate broad-band Raman through four wave mixing process inside an high-finesse cavity, it is necessary a specially designed mirror coatings to compensate the gas dispersion. Here we have selected a pair of cavity mirrors that can compensate the dispersion introduced by the Raman active medium, in a finite frequency region. Both the mirrors group delays are sufficiently smooth and low. Figure C.1 represents the cavity mirrors group delay dispersion (GGD).

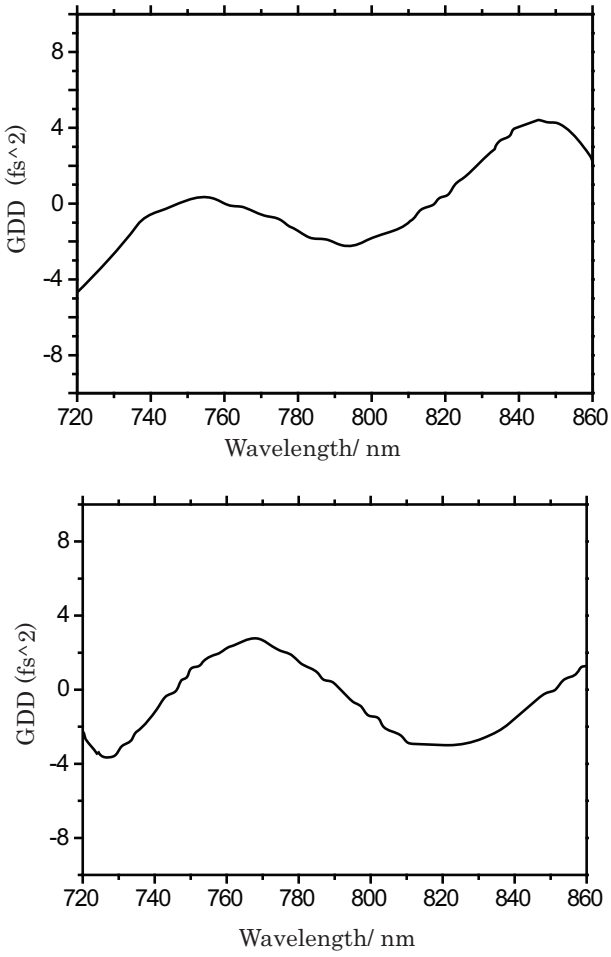

Figure C.1: Group delay dispersion of the cavity mirrors under one reflection

List of Publications

1. **Trivikramarao Gavara**, Takeru Ohashi, Yusuke Sasaki, Takuya Kawashima, Hiroaki Hamano, Ryo Yoshizaki, Yuki Fujimura, Kazumichi Yoshii, Chiaki Ohae, and Masayuki Katsuragawa, "Dual-frequency injection-locked continuous-wave near-infrared laser", Opt. Lett. **41**(13) 2994-2997 (2016)

2. Nurul Sheeda Suhaimi, Chiaki Ohae, **Trivikramarao Gavara**, Ken'ichi Nakagawa, Feng Lei Hong and Masayuki Katsuragawa, "Generation of five phase-locked harmonics by implementing a divide-by-three optical frequency divider", Opt. Lett. **40**(24), 5802-5805 (2015)

3. Chiaki Ohae, Nurul Sheeda Suhaimi, **Trivikramarao Gavara**, ken'ichi Nakagawa, Feng-Lei Hong, Masayuki Katsuragawa, "Frequency division in the optical frequency region and generation phase-locked high harmonics", Laser Society of Japan, The Review of Laser Engineering, **43**(8), 517-520 (2015).

4. Chiaki Ohae, Kazumichi Yoshii **Trivikramarao Gavara**, Masayuki Katsuragawa,"Arbitrary manipulation of amplitude and phase of a broadband coherent radiation with a highly-discrete spectrum", Laser Society of Japan, The Review of Laser Engineering, **45**(6), 319-323 (2017).

Proceedings

5. Nurul Sheeda Suhaimi, Chiaki Ohae, **Trivikramarao Gavara**, Ken'ichi Nakagawa, Feng-Lei Hong, and Masayuki Katsuragawa, "Generation of five phase-locked harmonics in the continuous wave regime and its potential application to arbitrary optical waveform synthesis", Proceedings of Third International Conference on Applications of Optics and Photonics (SPIE conference), PAPER NUMBER: AO100-7, Faro, Portugal, 8 - 12 May (2017)

Conference contributions-International

1. **T. Gavara**, C. Ohae, K. Nakagawa, K. Minoshima, and M. Katsuragawa: "Injection-locked tunable continuous-wave laser and its application to generation of ultrafast pulses above 100-THz repetition rate", 26th International Laser Physics Workshop (LPHYS'17), Kazan E K Zavoisky Physical-Technical Institute, Kazan, Russia, July 17–21, (2017). *Oral* **(Invited Talk)**

2. C. Ohae, N. S. Suhaimi,**T. Gavara**, K. Nakagawa, F. -L. Hong, K. Minoshima, and M. Katsuragawa, "Ultrafast Pulse Train at 125-THz Repetition Rate in the CW Regime", Nonlinear Optics (NLO2017), Session: Laser Sources, Waikoloa Beach Marriot Resort & Spa, Hawaii, United States, 17 – 21, July (2017). *Oral*

3. C. Ohae, N. S. Suhaimi, **T. Gavara**, K. Nakagawa, F. -L. Hong, K. Minoshima, and M. Katsuragawa, "Ultrafast Pulse Train with a repetition rate above 100 THz in the continuous-wave regime", The 24th Congress of the International Comission for Optics (ICO-24), Keio Plaza Hotel, Tokyo, Japan, 21 – 25, August (2017). *Oral*

4. **T. Gavara**, C. Ohae, and M. Katsuragawa, "Study and Development of Continuous-Wave Laser Based 10 THz Molecular Modulator", The fourth MIPT-LPI-UEC Joint Workshop on Atomic, Molecular, and Optical Physics. UEC, Tokyo, Japan, 25-29, March (2017). *Poster*

5. Nurul Sheeda Suhaimi, Chiaki Ohae, **Trivikramarao Gavara**, Ken'ichi Nakagawa, Feng-Lei Hong, and Masayuki Katsuragawa, "Generation of five phase-locked harmonics in the continuous wave regime and its potential application to arbitrary optical waveform synthesis", Third International Conference on Applications of Optics and Photonics (SPIE conference), PAPER NUMBER: AO100-7, Faro, Portugal, 8 - 12 May (2017) *Oral*

6. C. Ohae, N. S. Suhaimi,**T. Gavara**, K. Nakagawa, F. -L. Hong, K. Minoshima, and M. Katsuragawa," Generation and application of five phase-locked har-

monics in the continuous wave regime", VI International Conference "Frontiers of Nonlinear Physics", Nizhny Novgorod, Russia, July 17 - 23 (2016). *Oral* **(Invited Talk)**

7. C. Ohae, N. S. Suhaimi, **T. Gavara**, K. Nakagawa, F. -L. Hong, K. Minoshima, and M. Katsuragawa, "Generation and application of five phase-locked harmonics in the continuous wave regime", CLEO/QELS 2016, CLEO Technical Digest, JTu5A.83, San Jose Convention Center, San Jose, California, USA, June 5 - 10 (2016). *Poster*

8. **T. Gavara**, Y. Fujimura, R. Yoshizaki, T. Kawashima, T. Ohashi, Y. Sakaki, H. Hamano, K. Yoshii, and M. Katsuragawa, "Multiple frequency injection locked CW Ti:sapphire laser with a variable two frequency separation and power", ALPS p14-12, 4th advanced lasers and photon sources, Japan, (2015). *Poster*

9. N.Sheeda, C. Ohae,**T. Gavara**, K. Yoshii, and M. Katsuragawa, "Optical frequency divider and its application in ultra-broadband Raman comb", The second international workshop MIPT (Moscow, Russia) – UEC (Tokyo, Japan): atomic, molecular and optical physics. UEC, Tokyo, Japan, 16-21, October (2014). *Oral*

10. **T. Gavara** and M. Katsuragawa "Raman comb generation with Continuous Wave Laser", The first international workshop MIPT (Moscow, Russia) – UEC (Tokyo, Japan): atomic, molecular and optical physics. MIPT, Moscow, Russia, 30, October -1, November (2013). *Oral*

Conference contributions-Domestic

1. **T. Gavara**, T. Ohashi, Y. Sasaki, T. Kawashima, H. Hamano, R. Yoshizaki, Y. Fujimura, K. Yoshii, C. Ohae and M. Katsuragawa, "Dual Frequency Injection locked Continuous Wave Ti: SapphireLaser", 15pKJ-1, 71st spring meetings of the Japanese society of Physics Japan, (2016). *Oral*

2. Ryo Yoshizaki, **Gavara Trivikramarao**, Yuki Fujimura, Masayuki Katsuragawa, "Output stabilization of dual frequency injection locked continuous wave Ti: Sapphire laser", 14a-A13-2, 62nd spring meetings of the Japan Society of Applied Physics, Japan, (2015). *Oral*

3. **T. Gavara**, Y. Fujimura, R. Yoshizaki, N. S. Suhaimi, T. Kawashima, T. Ohashi, Y. Sasaki, H. Hamano, K. Yoshii, S. Uetake and M. Katsuragawa, "Dual Frequency Injection locked Continuous Wave Ti: SapphireLaser", 14a-A13-2, 75th spring meetings of the Japan Society of Applied Physics, Japan, (2014). *Oral*

4. Yuki Fujimura, **Gavara Trivikramarao**, Ryo Yoshizaki, Takuya Kawashima, Takeru Ohashi, Yusuke Sasaki, Hiroaki Hamano, Kazumichi Yoshii, Satoshi Uetake and Masayuki Katsuragawa "Developmentof a dual-frequency injection-locked continuous-wave Ti:Sapphire laser", 34th Annual meeting of laser society of Japan, (2014). *Oral*